NOTICE

The quality of this microform is heavily dependent upon the quality of the original thesis submitted for microfilming. Every effort has been made to ensure the highest quality of reproduction possible.

If pages are missing, contact the university which granted the degree.

Some pages may have indistinct print especially if the original pages were typed with a poor typewriter ribbon or if the university sent us an inferior photocopy.

Reproduction in full or in part of this microform is governed by the Canadian Copyright Act, R.S.C. 1970, c. C-30, and subsequent amendments.

AVIS

La qualité de cette microforme dépend grandement de la qualité de la thèse soumise au microfilmage. Nous avons tout fait pour assurer une qualité supérieure de reproduction.

S'il manque des pages, veuillez communiquer avec l'université qui a conféré le grade.

La qualité d'impression de certaines pages peut laisser à désirer, surtout si les pages originales ont été dactylographiées à l'aide d'un ruban usé ou si l'université nous a fait parvenir une photocopie de qualité inférieure.

La reproduction, même partielle, de cette microforme est soumise à la Loi canadienne sur le droit d'auteur, SRC 1970, c. C-30, et ses amendements subséquents.

Canada

DEVELOPMENT OF AN EXTRACELLULAR VOLTAGE CLAMP TECHNIQUE

by

Youmin Zhang

B.Sc., Shanghai University of Science and Technology,

Shanghai Second Medical School, Shanghai, People's Republic of China, 1988

THESIS SUBMITTED IN PARTIAL FULFILLMENT OF

THE REQUIREMENTS FOR THE DEGREE OF

MASTER OF SCIENCE

in

School of Kinesiology

SIMON FRASER UNIVERSITY

March 1992

ISBN 0-315-83713-6

APPROVAL

Name: Youmin Zhang

Degree: Master of Science

Title of thesis: Development of an Extracellular Voltage Clamp Technique

Examining Committee:

Chair: Dr. Igor Mekjavic

Dr. Tom Richardson
Senior Supervisor

Dr. Parveen Bawa

Dr. R.H.S. Hardy
External Examiner
School of Engineering Science
Simon Fraser University

Date Approved: April 15, 1992

PARTIAL COPYRIGHT LICENSE

I hereby grant to Simon Fraser University the right to lend my thesis, project or extended essay (the title of which is shown below) to users of the Simon Fraser University Library, and to make partial or single copies only for such users or in response to a request from the library of any other university, or other educational institution, on its own behalf or for one of its users. I further agree that permission for multiple copying of this work for scholarly purposes may be granted by me or the Dean of Graduate Studies. It is understood that copying or publication of this work for financial gain shall not be allowed without my written permission.

Title of Thesis/Project/Extended Essay

Development of an Extracellular Voltage Clamp Technique

Author:

(signature)

Youmin Zhang

(name)

April 15, 1992

(date)

Abstract

Epilepsy is a common brain disorder affecting approximately 0.5% of the world population. It is characterized by discrete episodes of abnormal brain activity and loss of consciousness referred to as seizures. It is known that seizures result from synchronous and excessive discharge of a population of hyperexcitable neurons within an epileptic focus. Previous studies have shown that both synaptic and non-synaptic mechanisms may underlie seizure activity. It is thought that one of the non-synaptic mechanisms, known as ephaptic interactions, may play a significant role in the generation and spread of epileptic seizures especially in CA1 area of the hippocampus. To investigate the role of ephaptic interactions in epileptic seizures, a voltage clamp circuit is required to manipulate the potentials in the extracellular space of brain tissue. This project developed a voltage clamp technique for clamping potentials and generating voltage gradients in artificial cerebral spinal fluid (ACSF), and investigated theoretical and practical problems associated with the use of this technique. The following phases were involved to achieve this goal.

The first phase of the project characterized the field potential distribution within a conductive medium based on the well-established properties of electric current. Potential profiles were developed for specific current sources including a point source and a wire source. These profiles were compared in order to determine the best approach for an extracellular voltage clamp. In the second phase of the project, a voltage clamp circuit was designed, constructed and tested on the bench. The circuit was based on an operational amplifier with a feedback loop.

After the successful debugging and evaluation of the voltage clamp circuit on the bench, it was tested in ACSF solution. Theoretical predictions for field potential

distributions were confirmed in the solution and voltage gradients were generated with a multi-channel voltage clamp system. A number of technical problems were met and overcome in these experiments. One major problem was caused by electrode polarization which could lead to circuit offsets and instability. To avoid this problem, the amount of current was kept as low as possible, and the time period for passing current was also limited. An integrator was used to correct the voltage offset and drift in the circuit.

Based on Ohm's law, the potentials drop by 1/r in a point current source field with a surrounding conductive medium, while the potentials in a wire source field drop by ln(1/r) (where r is the distance from the point source or the center of wire source). Cable theory suggests that the potential in a cable decays exponentially along its longitudinal axis with an electrotonic length λ. However this characteristic can be ignored for short silver wires in ACSF since its λ is much greater than 10 times the wire length of the wire used in this study. The recorded data from the point and wire current source field measurements was well correlated to the theoretical predictions. Experiments with either two channel or three channel voltage clamp system suggested that a stable and approximately linear potential distribution could be generated with a wire current source electrode. The results also showed that the voltage clamp system was still capable of maintaining the clamped voltages at the electrode tips even when a perturbing signal was involved, but the potentials between the tips were affected by the perturbing signal. The results of these experiments suggest that an array of closely spaced wire electrodes should be capable of clamping the extracellular space.

Acknowledgements

At the time I finish my project, I would like to thank Dr. Tom Richardson, my senior supervisor, who contributed tons of his energy to the formation of my personal characteristics as a successful scientific research student, and tried very hard to pull me back to the right track of thinking. Acknowledgements are also extended to Bob Richardson, for his continuous assistance in understanding the fundamental principles of an electronic circuit; Mr. John Fitz-Clarke for his contributions in the ideas of mathematical derivations; Mr. Mel Frank for his patient and enthusiastic attitude of supplying hardware components for the project; Ms. Collette O'Reilly, for her sincere guidance in the experiment set-up. Finally, special thanks should be given to Kevin Loken for his assistance in formatting the document of this thesis. It is really my hope that you can think of these people when you read my thesis.

Table of Contents

List of Tables

List of Figures

CHAPTER 1 INTRODUCTION

1.1 Background

1.1.1 Epilepsy

Epilepsy is an important focus of clinical and neurophysiological research. It is a remarkably common brain disease affecting one to two million people in the United States and twenty to forty million worldwide (Delgado-Escueta *et al* ., 1986). It is a functional brain disorder caused by synchronous and excessive neuronal discharge resulting from various intracranial or extracranial causes. It is characterized by discrete episodes, called seizures during which there is a disturbance of movement, behavior, sensation, perception and/or consciousness including absences, bilateral myoclonus, affective symptoms, and automation (Suthorland and Eadie, 1980). Pathophysiologically, an epileptic seizure is associated with the synchronous and excessive discharge of a large population of hyperexcitable neurons. The hyperexcitability is thought to be caused by an imbalance between inhibition and excitation of neuronal membranes. This imbalance leads to an enhanced neuronal excitability (Jackson, 1870; Futamachi and Prince, 1975; Andersen *et al*., 1978; Noebels and Prince, 1978; Wong and Prince, 1978, 1979; Andersen and Rutledge, 1979; Cutler and Young, 1979; Dingledine and Gjerstad, 1980). The epileptic focus is defined as a large aggregate of highly unstable neurons in a hyperphysiological state (Jackson, 1870).

Because of its wide variety of symptoms and the lack of long term effective treatment, epilepsy has attracted many neuroscientists to devote themselves to investigating the basic mechanisms of epilepsy. The search for new methods of diagnosis, control and

treatment of this disease involves molecular and cellular biology, neurochemistry and electrophysiology.

1.1.2 Mechanisms of epileptic seizures

Since epileptic seizures are thought to be related to an excessive discharge of a population of neurons, it seems likely that the mechanism is based on neuronal interactions. It is generally accepted that a positive feedback is involved in the generation and spread of epileptic seizures. This feedback may be via chemically mediated synaptic interactions and/or non-synaptic interactions.

A) Chemically mediated synaptic interactions

It is believed that chemically mediated synaptic interactions between neurons play an important role in the generation and spread of epileptic seizure. Activity produced in an epileptic focus can recruit synchronous discharge of adjacent neurons through synaptic transmission. Suppose three excitable cells A, B, and C are interconnected with excitatory synapses. If cell A fires, it will tend to excite cell B and C through synaptic interactions. Increased discharge in B and C can re-excite cell A. This re-excitation may eventually cause overdischarge of this population of neurons.

However, a number of reports suggested that epileptic activity can occur even during complete blockade of synaptic transmissions. Taylor and Dudek (1982; 1984a,b) and, independently, Jefferys and Haas (1982) observed a remarkable synchronization of population spike activity in hippocampal slices exposed to an artificial CSF with no Ca^{2+} ions. Under this condition, synaptic transmission was blocked because influx of Ca^{2+} is required for neurotransmitter release (Kandel and Schwartz, 1985). This finding suggests

that non-synaptic interactions may be involved in epileptiform activities. Three possible non-synaptic mechanisms are considered in the following sections: (1) Change in extracellular ionic concentration, (2) Electrotonic conduction through gap junctions, and (3) Ephaptic interactions.

B) Non-synaptic interactions

Changes in extracellular ionic concentrations is the first possible factor accounting for seizure activity. For the low extracellular Ca^{2+} model of epilepsy, in which chemical synapses are blocked, there is a transient elevation of extracellular K^+ ions during each spontaneous epileptic burst. This may contribute to neuronal excitability during the burst since the elevated K^+ concentration will alter the Nernst potential, moving the membrane potential closer to the firing threshold, and thus increasing the neuronal excitability. However the change in extracellular K^+ concentration usually occurs after the start of seizure discharge, so ion diffusion is probably not responsible for the rapid spread of seizure activity, but may contribute to seizure activity once initiated (Yaari, Konnerth and Heinemann, 1986). The second factor is electrotonic conduction through a gap junction. A gap junction is a specialized 2-4 nm diameter channel connecting two excitable cells. Unlike a chemical synapse, the cytoplasm of the two cells is continuously distributed via a gap junction channel. Because of its low electrical resistance, current can flow directly from one cell to the other. In this way, activities generated in one cell could propagate to the coupled cell and result in the spread of seizure discharge. However, electron microscopic studies indicate that gap junctions are not common in the mammalian cortex and are especially infrequent between the pyramidal cells in CA1 area of a hippocampus where low Ca^{2+} bursts are observed (Taylor and Dudek, 1982; Taylor *et al.*, 1984). Therefore, it seems unlikely that electrotonic coupling plays a major role in low calcium bursting.

Of great interest is the third kind of non-synaptic interaction, which is the ephaptic interaction and its possible role in epilepsy. An ephaptic interaction is defined as a direct electric influence of extracellular current flow on the excitability of neurons. This mechanism is illustrated in Figure 1.1. Field effects occur when the extracellular current (from source to sink in the figure), generated by the discharge of an active neuron, enters the intracellular space of a nearby passive neuron and fires it. This process can lead to depolarization of a population of cells exposed to extracellular current flow.

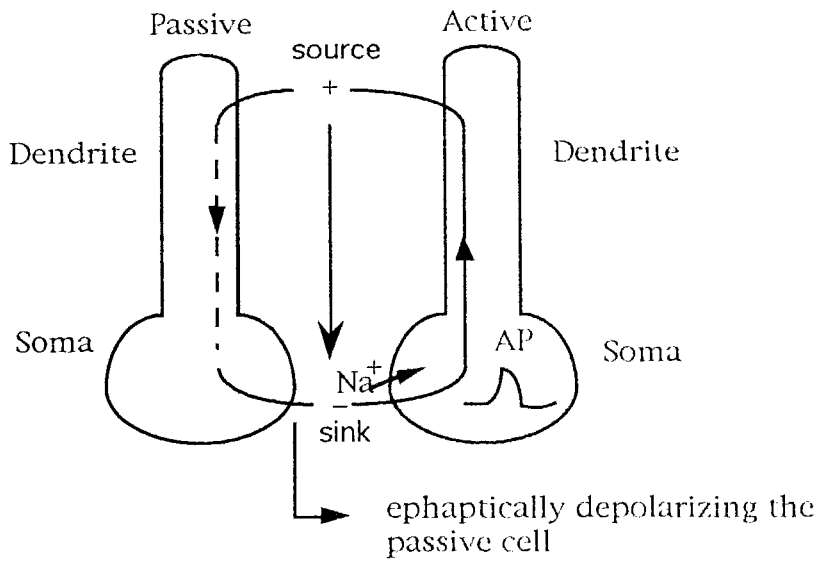

Figure 1.1 Ephaptic interactions Sodium current (Na^+) into an active neuron in an area of brain tissue will depolarize the neuron and generate an action potential (AP indicated in the diagram) in the soma. An extracellular current (source and sink shown in the diagram) produced by the discharge of this active cell can depolarize nearby cells, since a portion of the current will pass within its dendrosomatic axis. This effect of an extracellular field on the excitability of a passive cell is called ephaptic interactions or field effects.

The first demonstration that direct electrical interactions can take place between neurons came from Arvanitaki (Arvanitaki, 1942). Arvanitaki's experiment brought two axons in close proximity with one another in CSF. She observed that the propagation of an action potential down one axon could trigger an action potential in the other fibre, despite the lack of any physical contact between the two fibres. Arvanitaki called the juncture thus

formed an ephapse and hypothesized that analogous electrical stimulation was taking place at the ephapse.

C) Ephaptic interactions and epileptic seizures

Previous studies of ephaptic interactions have shown that they contribute to stimulus induced depolarization of CA1 pyramidal cells of hippocampal slices, and may cause synchronization and recruitment of neuronal discharge in the low [Ca^{2+}] model of epilepsy (Richardson *et al.*, 1984; Haas and Jefferys, 1984; Taylor and Dudek, 1984a,b). Epileptic seizures are characterized by a series of large amplitude field potentials, and it is thought that these field potentials may contribute to seizure activity through field effects (Konneth, Heinemann and Yaari, 1986). For example, extracellular electrical fields produced by one active population of neurons A can excite its neighboring passive population of neurons B, and the field effects generated by B could in turn affect A. This positive feedback loop may ultimately activate a group of neighboring subthreshold neurons and thus account for hyperexcitability (Turner *et al.*, 1984).

The hippocampal pyramidal layer is a likely site for ephaptic interactions because of the close packing and regular alignment between cell bodies, and the relative absence of intervening neuroglia (Taylor *et al.*, 1984). It is also notable that, of many structures in brain, the hippocampus is the most prone to seizures. Furthermore, the potentiation of CA1 population spikes during paired pulse or frequency stimulation is associated with a corresponding increase in ephaptic depolarization of CA1 pyramidal cells (Turner *et al.*, 1984). Other experiments have also demonstrated that externally applied electrical gradients as low as 5-10mV/mm can modify the excitability of dentate granule cells, whereas evoked potentials can generate a voltage gradient along the dendro-somatic axis as high as

100mV/mm. It therefore seems likely that extracellular fields are significant determinants of neuronal excitability in the hippocampus (Jefferys 1981; Richardson, *et al.*, 1984).

In order to experimentally investigate the role of ephaptic interactions in epileptic seizures, it is necessary to manipulate extracellular field potentials. It was proposed that a voltage clamp technique be developed for manipulating extracellular field potentials.

1.2 Voltage Clamp Technique

The voltage clamp technique is a powerful tool in electrophysiological research, especially in the study of membrane properties of excitable cells (Smith *et al.*, 1985). The basic idea of a simple voltage clamp circuit is to maintain the region near the tip of a recording electrode at a specific value of potential by varying the magnitude of current injected by the circuit. The control element is often an operational amplifier configuration to generate negative feedback (Figure 2.16). In order to avoid errors introduced by a voltage drop across the high resistance of microelectrodes, most simple voltage clamp circuits use a separate current passing and voltage sensing electrode.

1.3 Present Study

In order to generate artificial field potentials in the ACSF, an array of individual voltage clamp electrodes is required. At this time, there is no information available to help determine the appropriate category of electrodes or the magnitude of current required to successfully clamp a region within a fluid volume. Furthermore, it is not clear if several closely spaced electrodes with independent control circuits will remain stable. The objective of the present project is to help resolve these problems by 1) investigating the basic issues of current flow in a resistive medium using well-established theory, 2) designing,

constructing and bench testing a practical voltage clamp circuit, and 3) evaluating this circuit in ACSF using various configurations including a three channel voltage clamp array. The results are of direct value in further development of a practical extracellular voltage clamp technique.

CHAPTER 2 THEORETICAL BACKGROUND

The ultimate objective of the project is to develop a technique to generate a near linear potential distribution in a solution with a voltage clamp system. This chapter introduces the theoretical basis for field potential distributions using point and wire current sources and then describes the development of a basic voltage clamp circuit.

2.1 Theoretical Basis for Field Potential Distribution in a Conductive Medium

2.1.1 Single point source field

A glass micropipette passing current through a volume of ACSF to a distant distributed ground could be modelled as a single point current source in a conductive medium with a distant spherical ground, as shown in Figure 2.1. The constant current i originating from the source will spread in three dimensions to the distant grounded sphere.

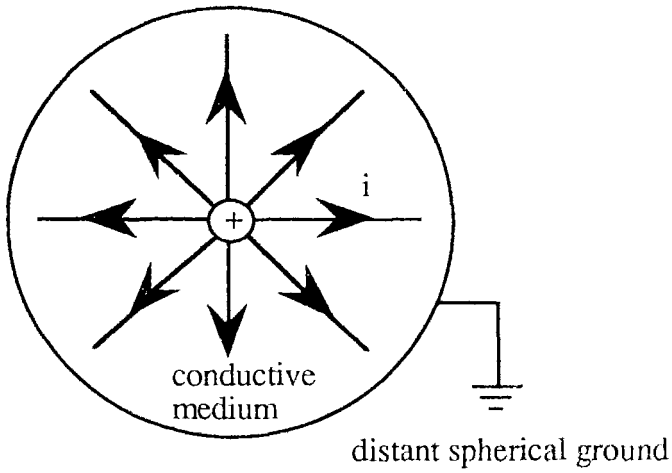

Figure 2.1 Electric field of a single point current source A single point current source (+) with constant current i is in a conductive medium with a distant spherical ground. The constant current i spreads from the source in 3 dimensions to the ground.

If the conductive medium is purely resistive, then Ohm's law (Scott, 1959) leads to the following derivation of potentials in the medium. Consider an infinitesimal spherical shell of thickness dr (from r to r+dr); the resistance of this shell dR is given by

$$\begin{aligned} dR &= \rho \cdot \frac{dr}{A} \\ &= \rho \cdot \frac{dr}{4\pi r^2} \\ d\Phi &= i \cdot dR \\ &= i \cdot \rho \cdot \frac{dr}{4\pi r^2} \\ \int d\Phi &= \frac{i\rho}{4\pi} \cdot \int \frac{dr}{r^2} \\ \Phi &= \frac{i\rho}{4\pi} \cdot (-\frac{1}{r}) + C \\ &= K \cdot \frac{1}{r} + C, \end{aligned} \qquad (2.1)$$

where

r ≡ the distance of a sphere in the medium from the center of the source;

ρ ≡ the resistivity of the conductive medium;

R ≡ the resistance of the medium ranging from the edge of the source to the sphere of distance r;

Φ ≡ the potential at the sphere of distance r;

K ≡ - iρ/4π, which is a constant determined by the source and the properties of the medium;

C ≡ the constant determined by the boundary conditions.

If the edge potential of the source ($r = a_o$, the radius of the source) is V_o, and the ground is at infinity ($r \rightarrow \infty$, $\Phi=0$), these boundary conditions give

$$K = a_o V_o, \text{ and}$$
$$\Phi = \frac{a_o V_o}{r}. \qquad (2.2a)$$

If the ground is at a certain distance r_{gn}, then from Equation 2.1 the potential becomes,

$$\Phi = \frac{V_o}{1/a_o - 1/r_{gn}} \left(\frac{1}{r} - \frac{1}{r_{gn}}\right). \qquad (2.2b)$$

ACSF, an electrolytic solution, is a conductive medium with a certain resistivity. Therefore the equations 2.2a&b can be applied to predict the potential profile in ACSF under experimental conditions.

Plots of the potential distribution under a point current source are shown in Figure 2.2. The graphs A and B show the potential distribution generated by a point current source with an infinite and finite ground. Curve **A** with an infinite ground indicates a potential decay from V_o at the edge of the source (radius is a_o) to zero at infinity. The potential decays by 1/r, where r is the distance from the center of the source. If a ground is present at a finite place (r_{gn}=8 in the figure), potential curve **B** is shifted towards the source, and decays more dramatically but is still proportional to 1/r.

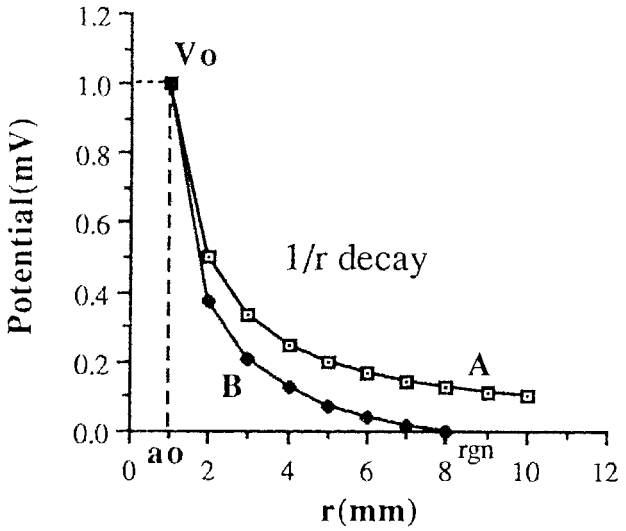

Figure 2.2 Single point source potential distribution with infinite or finite ground Curves A and B show potential distributions generated by a point current source with an infinite and finite ground, respectively. Curve A decays by 1/r with an infinite ground from V_o at the edge of the source (radius is a_o) to zero at infinity, where r is the distance from the source center. If the ground is located at a finite place (r_{gn}=8 in the figure), the potential (shown in curve B) shifts towards the source, but is still proportional to 1/r.

2.1.2 Single wire source field

A wire passing current through a volume of ACSF to a distant ground could be modelled as a wire spanning the depth of a disc shaped volume of conductive medium with a distant cylindrical ground around the perimeter of the disc as in Figure 2.3. Diagram A shows the top view of the wire, in which a constant current, i, spreads in two dimensions from center of the wire to a distant cylindrical ground. Diagram B shows the sideview with current flowing perpendicular to the wire.

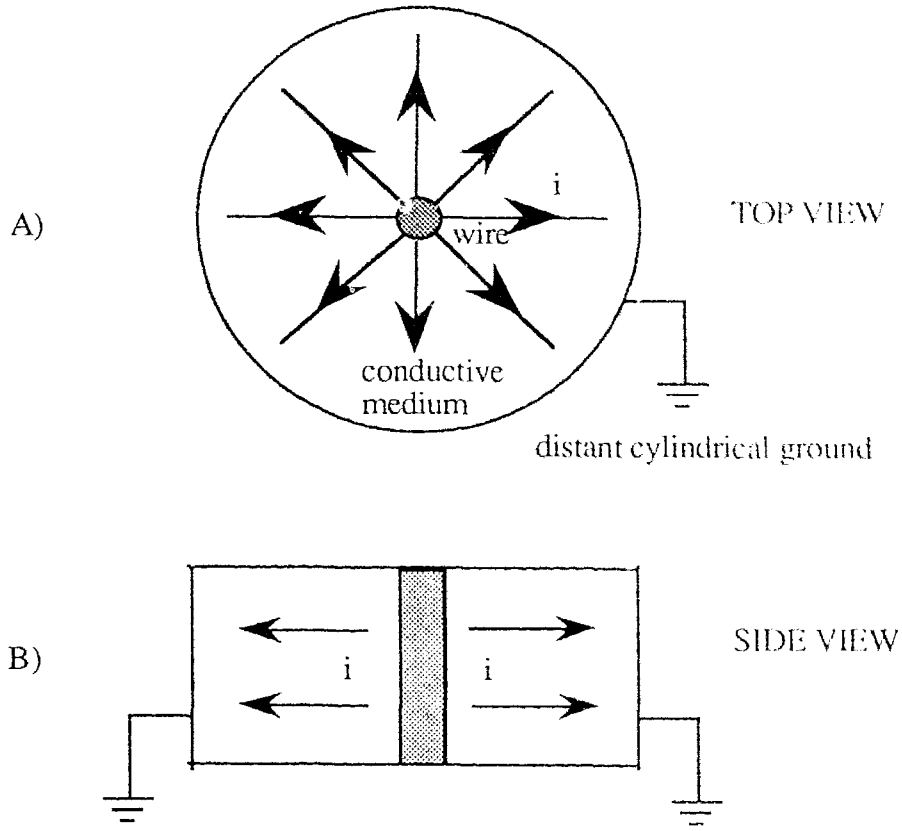

Figure 2.3 Configuration of a single wire current source Diagram A) and B) show top view and side view of a single wire in a conductive medium, in which a constant current i spreads in two dimensions from center of the wire to a distant cylindrical ground. The direction of current flow is perpendicular to the wire.

This configuration is made more complicated by the cable properties of the wire as shown in Figure 2.4A. As current passes through the wire, the amount of current decreases in both the longitudinal and radial axis (i_a). The end result is a gradual decrease in surface voltage along the length of the wire. The cable can be modelled as an electrically equivalent circuit as shown in Figure 2.4B. In this diagram, the wire is divided into many segments. For each unit segment, r_a is the axial resistance of the cable, r_{cw} is the radial cable wall resistance, and r_m is the radial resistance of the medium between the segment of the wire and the distant ground. At an axial distance g, the axial and the wall current are assumed to be i_{ag} and i_{wg}, and the voltage is V(g). Ground cylinder (GND) is placed at a finite place (r_{gn} is the distance of the ground from the center of the wire) in the external medium.

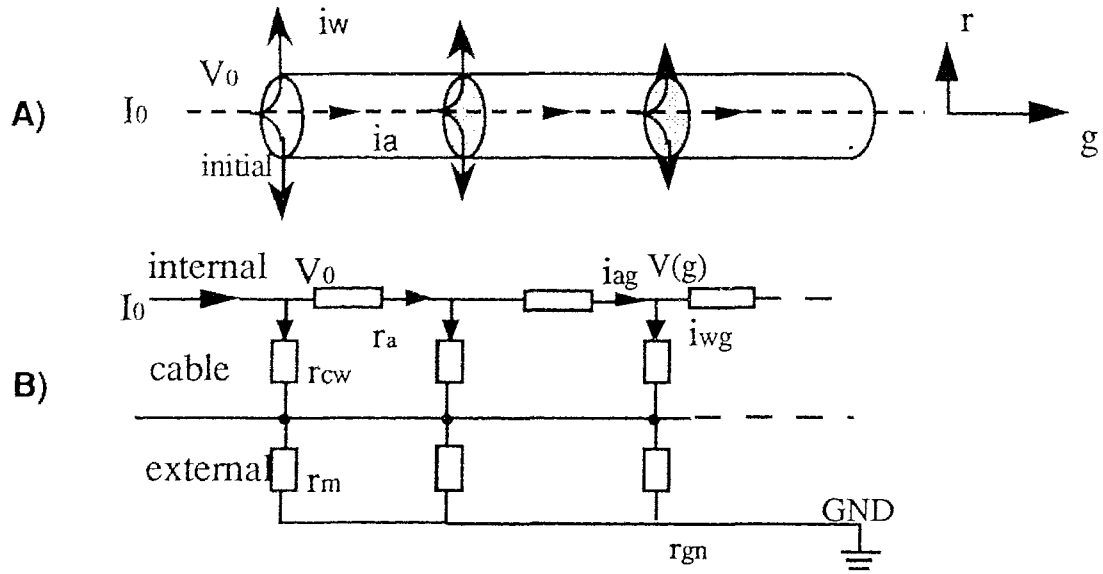

Figure 2.4 A single wire cable and its electrically equivalent circuit The drawing A shows a finite cable through which current is passing. The potential and current at the initial segment of the wire are V_o and I_o, respectively. As current passes through the wire, the amount of current decreases in both longitudinal and radial axis because of leakage current through the wall (i_w) and the voltage drop along the wire. The drawing B is an electrically equivalent circuit for the single wire within a conductive medium, where r_a is the resistance of each small segment along the cable axial direction, r_{cw} and r_m are the cable wall resistance and surrounding medium resistance of the segment, respectively. At a distance g, the axial and the wall current are assumed to be i_{ag} and i_{wg}, and the voltage is V(g). Ground cylinder (GND) is placed at a finite distance in the external medium (r_{gn} is the radial distance of the ground cylinder from the center of the wire).

Cable theory (Katz, B., 1966) indicates that the voltage drops exponentially along the cable, as in Equation 2.3 (derivations are in Appendix A). At one electrotonic length λ, the voltage will have dropped to 1/e or 36.8 percent of its driven voltage.

$$V(g)=V_o \cdot \exp(-g/\lambda), \qquad (2.3)$$

where

g $\equiv$ the axial distance variable from the initial part of the cable;

V_o $\equiv$ the initial potential of the wire;

λ $= \sqrt{(r_{cw}+r_m)/r_a}$, is the electrotonic length of the wire.

The voltage gradient of interest to this project is associated with current flow from the wire surface radially to the distant ground. For a single segment (Δg) of the wire at distance g (Figure 2.5), the potential ($V_{g,r}$) at distance r from the wire center is given by Equation 2.4 (derivations are in Appendix B).

$$V_{g,r} = \frac{V_o \cdot \exp(-g/\lambda)}{\ln(a_o/r_{gn})} \cdot \ln(r/r_{gn}), \qquad (2.4)$$

where

a_o ≡ the radius of the wire cable;

r_{gn} ≡ the radial distance of the ground cylinder to the center of the wire;

r ≡ the radial distance from the center of the wire;

$V_{g,r}$ ≡ the potential at distance r from the wire center in the plane of the segment Δg.

This equation indicates that the voltage decays in ln(1/r) in the plane perpendicular to the wire. However, if the voltage drop along the wire is substantial, then the voltage gradients will differ for each segment along the length of the wire. This is undesirable for a voltage clamp application where the objective is to clamp a volume to a specific voltage. The worst case voltage drop will occur if the cable wall resistance (r_{cw}) is zero and the wire length is infinite. If contamination or oxidation of the wire surface creates a resistive barrier or a significant resistance exists at the metal-electrolyte interface, then the wire will behave as if it were partially insulated and the voltage drop along its length will be less. Similarly if the wire has a finite length, voltage drop per unit length will also decrease since less current will be lost to axial flow.

The following section estimates λ for the silver wire planned for use in actual experiments in order to determine whether this wire will have a significant voltage drop along its length. These calculations are based on the worst case where cable wall resistance is zero and the voltage decays at the rate determined for an infinite cable. The first task is to derive the equation for resistance to current flow through the ACSF from the wire to the ground. A very small segment Δg (length h) of the wire is selected as shown in Figure 2.5, in which h is the length of the segment, a_o is the radius of the wire, and dr represents an infinitesimal distance between two cylinders in the medium, and finally i_{wg} is the radial wall current at the segment.

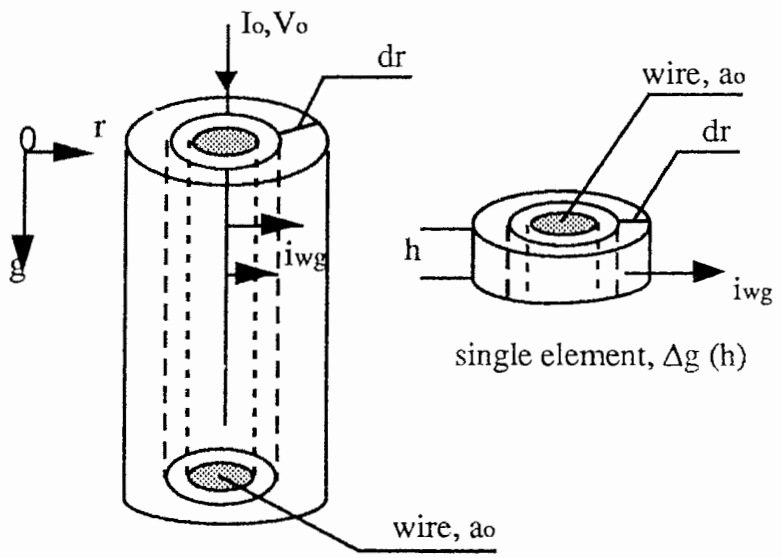

Figure 2.5 A small segment of a wire in ACSF medium This figure shows a long wire, indicated by the shaded outline, surrounded by ACSF. To the right a single element of the wire Δg is shown. For the single small segment Δg, h is the length of the segment, a_o is the radius of the wire, and dr represents an infinitesimal distance between two cylinders in the medium, and finally i_{wg} is the wall leakage current at the segment.

Medium resistance for a unit length of a wire in Equation 2.3 (r_m) is calculated based on the definition of resistance,

$$
\begin{aligned}
r_m &= R \cdot h \\
&= \left(\int_{a_o}^{r} dR \right) \cdot h \\
&= h \cdot \int_{a_o}^{r} d\left(\rho \cdot \frac{r}{A}\right) \\
&= h \cdot \int_{a_o}^{r} \frac{\rho}{2\pi r h} \cdot dr \\
&= \frac{\rho}{2\pi} \cdot \int_{a_o}^{r} \frac{dr}{r} \\
&= \frac{\rho}{2\pi} \ln \frac{r}{a_o}, \qquad (2.5)
\end{aligned}
$$

where

r_m ≡ medium resistance for a unit length of a silver wire (Ωcm);

R ≡ the medium resistance from the wire edge to the cylinder of segment Δg;

h ≡ the length of the segment Δg;

a_o ≡ the radius of the wire;

r ≡ the radial distance of the cylinder from the center of the wire;

A ≡ the round area of the cylinder for the segment Δg;

ρ ≡ the resistivity of ACSF.

Given that the silver wire has a radius a_o of 0.01cm, the ground distance (disk radius) r is 1cm, and the resistivity of ACSF ρ is approximately 20Ωcm, the medium resistance for a unit length cable r_m from Equation 2.5 is 14.66Ωcm. Given that the resistivity of silver is 0.162×10^{-7} Ωm (Scott 1959, p.186), the cable axial resistance per unit length r_a is,

$$r_a = \frac{R}{l}$$

$$= \frac{\rho}{\frac{1}{4}\pi d^2}$$

$$\approx 5.16 \times 10^{-3}\ (\Omega/\text{cm}), \qquad (2.6)$$

where

l ≡ the length of the wire;

R ≡ the resistance of a silver wire with length l;

ρ ≡ the resistivity of the silver wire ($0.162 \cdot 10^{-7}\ \Omega$m);

d ≡ the diameter of the silver wire (0.02cm);

r_a ≡ the axial resistance of the wire per unit length.

Based on these values, λ of the silver wire in ACSF is calculated using Equation 2.3 to be 53.3cm. This very large value indicates that the voltage drop along a 1mm wire (planned length) will be insignificant and can be ignored.

The plot in Figure 2.6 shows the expected potential distribution generated by a wire electrode assuming that V(g) is constant and that the wire extends the whole depth of the disc. The potential decay from V to zero at distance r_{gn} is proportional to ln(1/r) in the plane perpendicular to the wire. In the figure, r is the distance from the center of the wire, V is the voltage at the edge of the wire in that plane, and r_{gn} is the distance to ground.

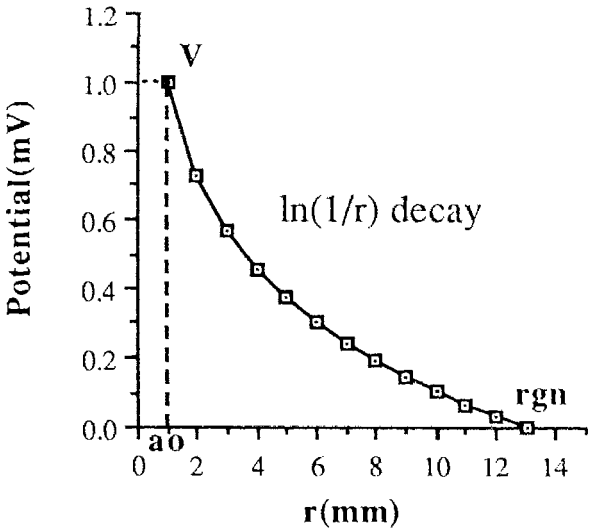

Figure 2.6 Potential distribution of a single wire source field This graph shows the potential distribution generated by a single wire source in the plane perpendicular to the wire. The wire is assumed to be isopotential along its length with a surface voltage of 1.0mV. The potential decay from V to zero is proportional to ln(1/r). In the figure, r is the distance from the center of the wire, V is the voltage at the edge of the wire, a_o is the radius, and r_{gn} is the distance to the ground cylinder.

2.1.3 Comparison of field potentials for a point source and a wire source

Comparison of the potential profiles of a single point source and a single wire source (Figure 2.5 and 2.6) reveals that the 1/r curve for the point source drops more quickly than the ln(1/r) curve when the same boundary conditions exist, as shown in Figure 2.7A. In terms of voltage clamping, a slower decay of potential is desirable. Therefore, the wire current source should be more effective than the point source. Figure 2.7B shows the ratio of the point curve versus the wire curve. The graph indicates a particular poor performance of the point source in the region halfway between the wire and ground. In this region, the voltage of the point source gradient is only half that for the wire source.

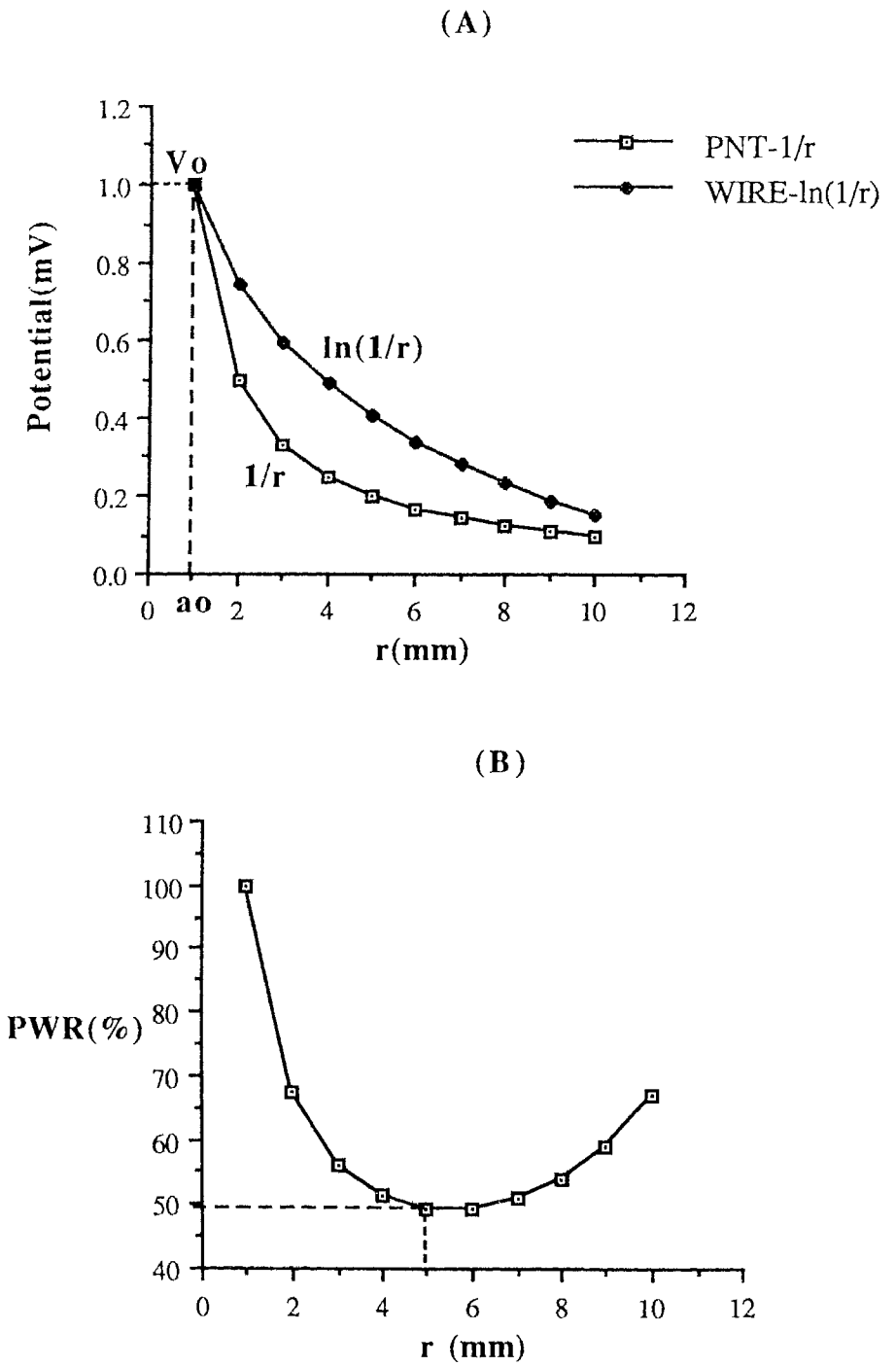

Figure 2.7 Comparison of point and wire source curves Graph A indicates a more rapid decay of the point curve than the wire curve under the same initial boundary condition (a_o =1, and V_o =1). Therefore, the wire source is better than the point source in terms of its voltage clamping. Graph B shows the potential ratio of the point curve versus wire curve (PWR is Point Wire Ratio). The plot indicates a poor performance of the point source in the region halfway from the wire to ground where the point source voltage is half that for the wire source.

2.1.4 Multiple point source field

In order to voltage clamp the ACSF, an array of closely spaced electrodes will be required. This section considers the issue of multiple current passing micropipettes. Consider two point sources I_1 and I_2, in a conductive medium a distance d apart with edge voltages V_1 and V_2. P is any point in the medium with distance r_1 and r_2 from I_1 and I_2, as shown in Figure 2.8.

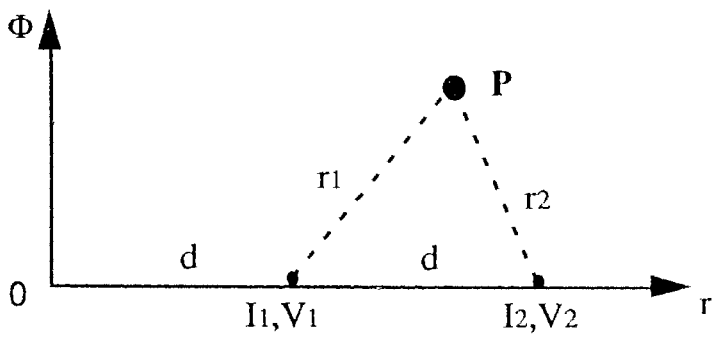

Figure 2.8 Two point sources I_1 and I_2 The figure shows two point sources I_1 and I_2 in a conductive medium with a distance d apart. P is any point which is r_1 and r_2 away from I_1 and I_2. V_1 and V_2 are edge voltages of the two sources.

Using the principle of superposition, the potential at point P should be the sum of potentials produced by the field of two single point sources I_1 and I_2 (Equation 2.1, assuming an infinite ground),

$$\Phi = \sum(K_i/r_i) \qquad (i=1,2), \qquad (2.7)$$

where

r_i ≡ the distance of point P from point source i, i=1, 2;

K_i ≡ a constant determined by boundary condition of current source I_i, i=1, 2.

The software package MathCAD was used to solve for K_i using different sets of boundary conditions. Figure 2.9 shows the potential distributed along the line joining 2 electrodes clamped to the same voltage. The electrodes are 30mm apart and the ground is at an infinite distance. The contributions from both electrodes are indicated by Φ1 and Φ2. Note the substantial voltage drop between the electrodes.

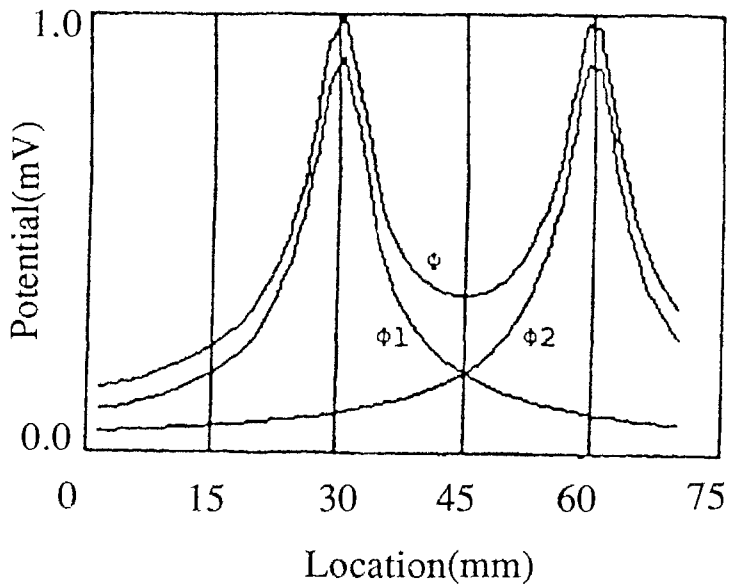

Figure 2.9 Potential distribution for two point sources Curve Φ shows the potential distribution generated by two point sources clamped to the same voltage and separated by 30mm. The ground is at an infinite distance. The curve Φ1 and Φ2 show the potential contributed by the individual electrodes.

If the same electrodes are clamped to opposite potentials, the voltage distribution shown in Figure 2.10 is obtained. The curve shows a roughly linear distribution between the electrodes.

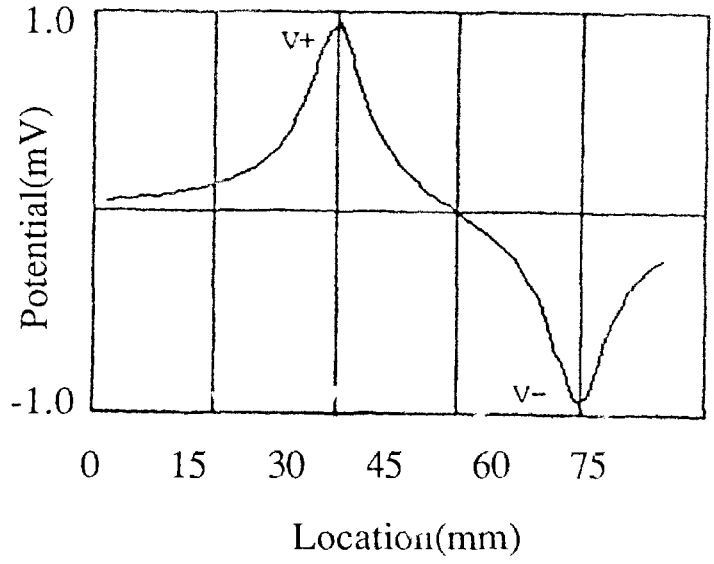

Figure 2.10 Potential distribution of two point sources clamped to opposite voltages Two opposite peak potentials (V+ and V-) are present at the two current source electrodes with a roughly linear potential distribution between the peaks.

2.1.5 Multiple wire source field

The following section considers the voltage profiles generated by multiple wire electrodes. Consider two parallel wires in a conductive medium, as shown in Figure 2.11. P is any point in a plane with coordinates x and y. The plane is perpendicular to the wires and has distance g from the initial segment of both wires. The distance of point P from the center of either wire is given by r_1 or r_2.

Similar to the multi-point source curve, the potential distribution for two wire current source can be obtained by using the principle of superposition:

$$\Phi(P) = \Sigma\left[\frac{V_o \cdot \exp(-g/\lambda)}{\ln(a_o/r_{gn})} \cdot \ln(r_i/r_{gn})\right] \quad (i=1,2)$$

$$= \frac{V_o \cdot \exp(-g/\lambda)}{\ln(a_o/r_{gn})} \cdot \ln\left[\Pi(r_i/r_{gn})\right], \qquad (2.8)$$

where

r_i ≡ the distance of point P from the center of either wire;

r_{gn} ≡ the distance for the common ground.

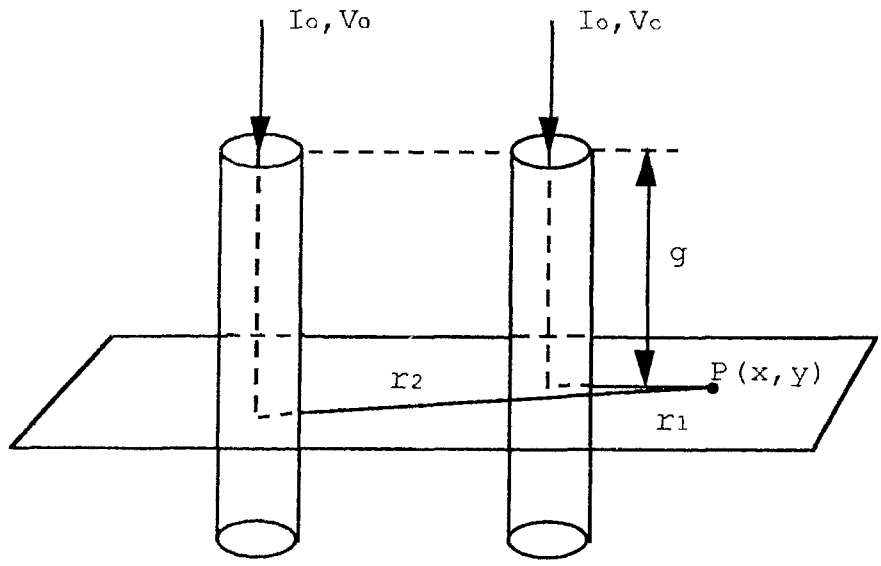

Figure 2.11 Two wire current sources Two long wires are placed parallel to each other with initial current and voltage I_o and V_o, respectively. P (with coordinates x and y) is any point in a perpendicular plane with distance r_1 and r_2 from the centers of both wires. The symbol g is the distance from the start of the wires to the plane.

A numerical solution to this equation was obtained using MathCAD software. Plots of the results are shown in Figure 2.12 for two wires clamped to the same voltage and Figure 2.13 for wires clamped to the opposite polarity. In Figure 2.12, Φ is the potential distribution generated by the two wire sources. It is the sum of the contribution from each source electrode shown as Φ1 and Φ2. Although similar in shape to the curve generated for two point sources, it has a smaller voltage drop between the electrodes. When the same electrodes are clamped to opposite potentials (Figure 2.13), an approximately linear potential is generated between the wires.

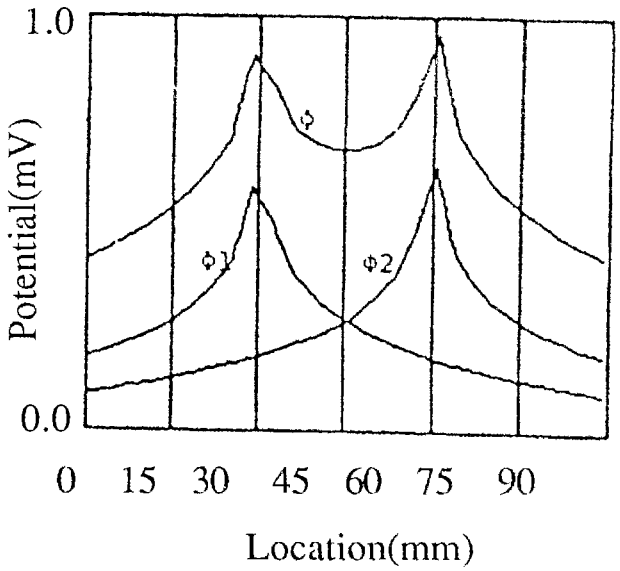

Figure 2.12 Potential distribution for two wire sources Curve Φ shows the potential distribution generated by two wire sources clamped to the same potential and separated by 30mm. The ground is at an infinite distance. The curves Φ1 and Φ2 show the potential contributed by the individual electrode.

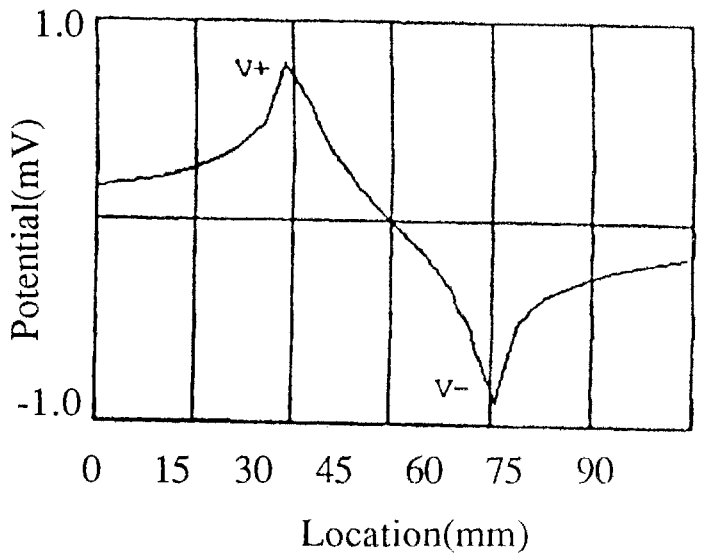

Figure 2.13 Potential distribution generated by two wire sources clamped to opposite voltages Two opposite peak potentials (V+ and V-) are present at the two wire sources with a roughly linear potential distribution between the peaks.

2.1.6 Comparison of field potentials generated by two point and wire sources

The objective of this project is to generate a specific voltage gradient in the ACSF by using multiple current passing electrodes. A comparison of potentials generated by a pair of point or wire current sources clamped to the same potential (Figure 2.14) indicates that there is a slower voltage decay for a wire source (ΦW). The maximum difference is halfway between the peaks as shown in Figure 2.14B. Figure 2.15 indicates that the wire source field also shows a more linear voltage gradient between the two current sources when they are clamped to opposite voltages.

Based on these results, a wire current source should be more appropriate for clamping the ACSF than a point source. The spatial arrangement of the current passing electrodes for generating a voltage gradient in an actual experiment largely depends on the magnitude of the voltage gradient and the voltages that can be clamped at each spot. Clearly, the electrodes should be placed as closed as possible to prevent any significant drop of potentials between the electrodes, either for clamping the voltages at different values as in Figure 2.15 or the same value as in Figure 2.14. The actual separation of the electrodes will be a compromise between the technical problems of large numbers of electrodes and the need to minimizing the inter-electrode distance.

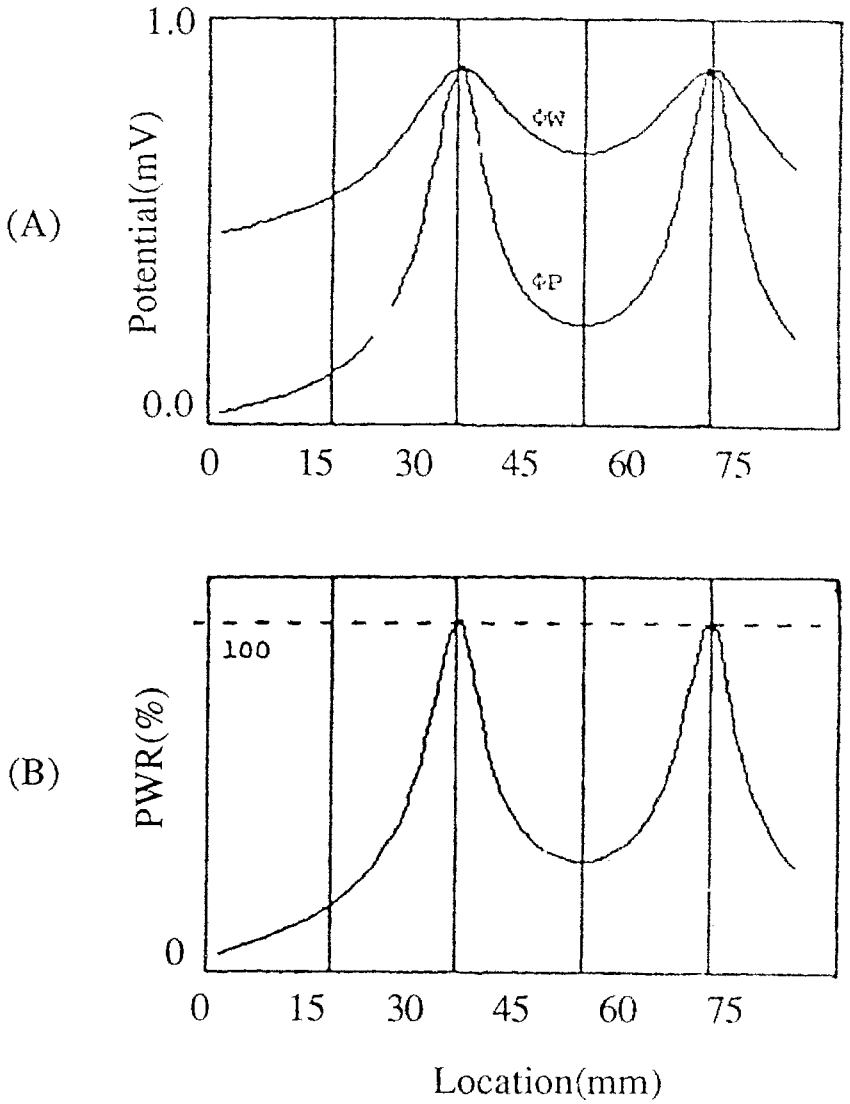

Figure 2.14 Comparison of field potentials generated by two point and wire sources clamped to the same potential Graph A indicates that the potential generated by a pair of wire electrodes ΦW has a shallower voltage drop between the current sources than the point electrodes ΦP. Graph B compares the profiles of the two electrode types by plotting ΦP as percentage of ΦW (PWR%).

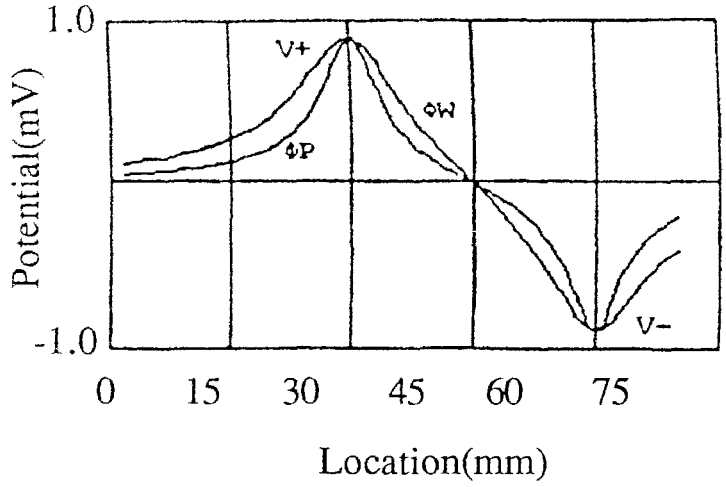

Figure 2.15 Comparison of field potentials generated by two point and wire sources clamped to opposite voltages The potential distribution between the electrodes is more linear for the wire electrodes (ΦW) than for the point electrodes (ΦP).

2.2 Voltage Clamp Technique

2.2.1 Concept of voltage clamp technique

The voltage clamp is one of the most powerful tools for studying the membrane properties of excitable cells. It can be used in experiments for the precise measurement of membrane ionic currents underlying excitation. This technique, which uses an electronic feedback to keep membrane potential unchanged during transient changes of membrane conductance, was originated by K.S. Cole in the late 1940s. Because the conductance changes that occur during electrical excitation of a nerve are completely controlled by the membrane potential and not by membrane current, the control of membrane potential is critical to investigating the time course of conductance changes. Cole's original idea of the voltage clamp was extended to clamp the action potential in a study of the electrical characteristics of the action potential in axons (Smith *et al.*, 1985).

In Cole's experiments with the voltage clamp in 1947, metallic microelectrodes were used for impaling squid axons. After the impalement, a step-like change in transmembrane potential was made in order to vary the current passing through the membrane. In these experiments, a single internal electrode was used for both recording potential and passing current. Since the current across the membrane may be large, the high and often variable resistance of the electrode introduced an error in measurement and often caused the circuit to be unstable (Smith *et al.*, 1985). The method can be improved if two electrodes are used, one for current passing, and one for voltage sensing. Thus, the resistance of the potential sensing microelectrode will not give rise to a voltage across the electrode since there is no current flow. The two electrode clamp is not always practical for neurons, but is certainly suitable for clamping the extracellular space.

The diagram of a prototype voltage clamp circuit is shown in Figure 2.16. It is a conceptual diagram showing an electronic circuit based on a simple operational amplifier (feedback amplifier, FBA) within a feedback loop. The requirement for equal input terminal signals of this ideal op-amp causes the amplifier to generate the appropriate current output to maintain the potential at the tip of the voltage sensing electrode (V_s) the same as V_{com}. The I_p and V_s electrode tips are placed as close as possible to each other in the tissue to minimize any voltage difference between the two electrode tips. By using separate current passing (I_p) and voltage sensing (V_s) electrodes, the amount of current passed will not affect the potential recorded by the V_s electrode, and the potential of the tissue at the location of the I_p electrode tip will be clamped at the desired voltage (V_{com}).

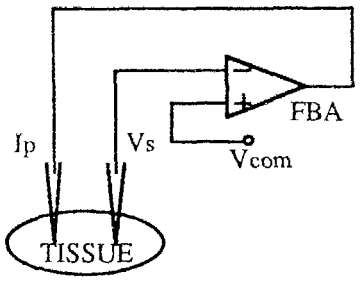

Figure 2.16 A simple voltage clamp circuit This is a conceptual diagram showing an electronic circuit based on a simple operational amplifier (feedback amplifier, FBA) within a feedback loop. The requirement for equal input terminal signals (+ and -) of this ideal op-amp makes the potential at the end tip of the voltage sensing electrode the same as V_{com}.

2.2.2 The voltage clamp circuit developed in the present study

Considering the specific requirements for voltage clamping the extracellular space in the study of ephaptic interactions, the prototype circuit (Figure 2.16) needs to be modified. Three extra parts were appended to the prototype of the voltage clamp circuit as shown in Figure 2.17. (1) An RC low pass filter (trimpot, TRM and capacitor C) was added so that the circuit could be tuned to clamp only the low frequency, widely distributed potentials usually associated with ephaptic interactions, rather than the high frequency fields of individual action potentials. (2) A high impedance follower (HIF) was added to assure that no current would pass through the V_s electrode. (3) A differential amplifier was appended for monitoring the current, I_p, required for clamping the target at a specific voltage.

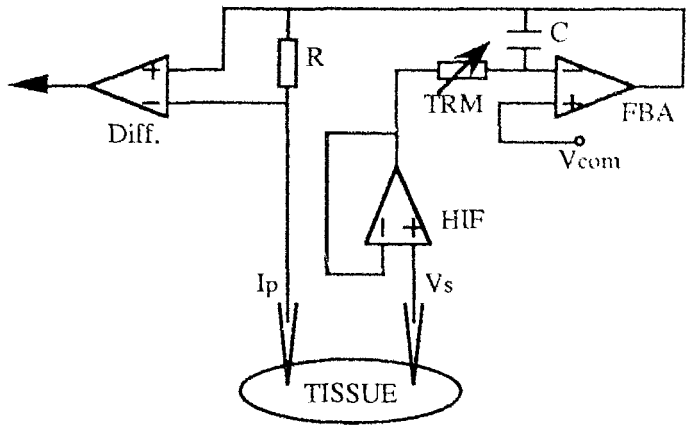

Figure 2.17 Extended voltage clamp circuit This is an extended voltage clamp circuit with three additional parts added to the circuit in Figure 2.16. (1) the trimpot (TRM) and capacitor C make up a low pass filter for clamping a signal of a frequency lower than the corner frequency of the filter. (2) A resistor (R) and differential amplifier (Diff in the diagram) are added to measure current output by the clamp. And (3) the voltage detected by V_s is buffered to stop current flow through the electrode.

Voltage clamp amplifiers for microelectrodes have been available since the mid 1970s. However, these clamps do not have the required filter properties described above. Commercial units are also very expensive, often costing more than 5,000 dollars, whereas the custom unit described above costs less than 50 dollars. It is, therefore, practical and economical to have a self designed and constructed voltage-clamp circuit system with multiple channels for the present project. A schematic of a single channel of the custom voltage clamp circuit is shown in Figure 2.18.

2.2.3 Bench test of voltage clamp circuit

The complex properties of microelectrodes in ACSF made it necessary to test the voltage clamp circuit on the bench before any experiments were carried out in ACSF. Since the extracellular space is resistive, a simple network of three resistors was used to simulate the various current paths between the electrodes and ground, as shown in Figure 2.18. A perturbing signal (V_{pt}) was input through resistor R_{pt} to simulate spontaneous

physiological signals which might be present within the extracellular space of hippocampal tissue.

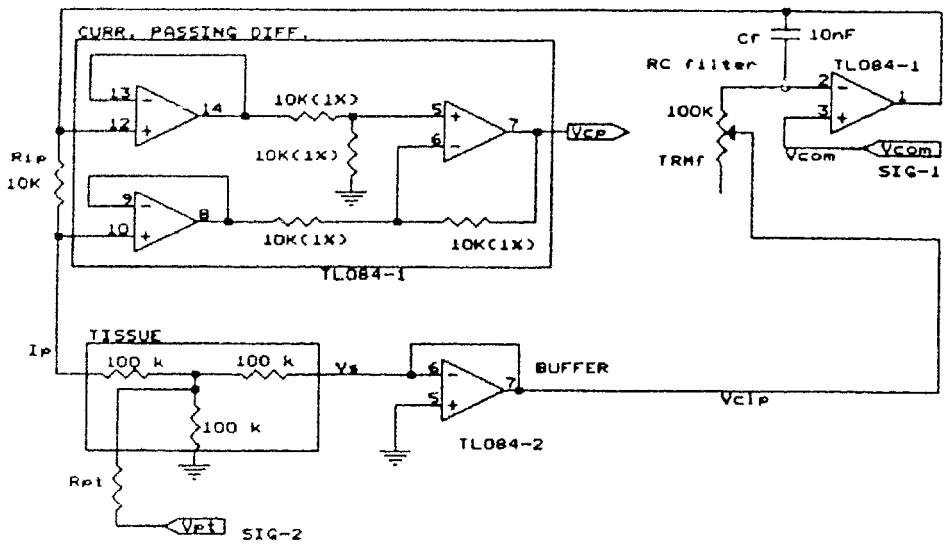

Figure 2.18 Bench Test of the voltage clamp circuit The schematic for the voltage clamp is shown with additional circuitry required for bench testing. Three resistors were used to simulate the resistivity of brain tissue. A perturbing signal (V_{pt}) was input through resistor R_{pt} to mimic spontaneous physiological signal which may occur within the extracellular space of live tissue. To test the clamp function of the circuit, clamp signal V_{clp} was compared with the command signal V_{com} during different perturbing signals.

The clamp circuit successfully maintain the voltage at V_s at the command voltage, V_{com}, during low frequency perturbations applied to V_{pt} with a gradual failure to clamp at the frequency of the perturbing signal approaching the corner frequency defined by the RC filter. The circuit also successfully followed low frequency changes in the command voltage. However, as the frequency of the command input was increased the RC filter caused a gain in the feedback loop resulting in a clamped voltage greater than the command voltage. Although not ideal, this property of the circuit will not limit its intended use in blocking field potentials generated by physiological activity. When the clamp is used to generate artificial field potentials, the command voltage will have to be filtered at a corner frequency below that of the clamp.

CHAPTER 3 METHODS

3.1 ACSF Solution

An artificial cerebral spinal fluid (ACSF) was made up of seven salts based on the following recipe (in mM) : NaCl 124, $NaHCO_3$ 26, KCl 3.5, NaH_2PO_4 1.4, $MgSO_4 \cdot 7H_2O$ 2.0, Glucose 10 and $CaCl_2$ 2.0. Since $CaCl_2$ can precipitate at a high pH, it was mixed with the solution after it was bubbled with $95\%O_2/5\%CO_2$ gas. The procedure of making ACSF constituted the following steps: 1) Approximately 50ml of water out of 230ml in a flask was placed in a small Petri dish. 2) The $CaCl_2$ was placed into the Petri dish and mixed well. 3) The other six salts in the recipe were weighed and dissolved into the water left in the flask. This solution was then bubbled with $95\%O_2/5\%CO_2$ for 3 minutes. 4) The $CaCl_2$ solution in the Petri dish was then added to the bubbled solution and volume was adjusted to 250ml by adding water.

3.2 Making Electrodes

In terms of materials and structure, there are two general categories of electrodes in neurophysiological research: metallic and fluid-bridge electrodes. Both electrodes were employed in this project for current passing, voltage sensing and voltage recording.

3.2.1 Ag-AgCl wire electrode

Silver wire electrodes must be coated with the salt silver chloride. This sheath of AgCl decreases polarization and resistance at the metal electrolyte interface by allowing current to be carried by Cl^- ions. The decreased polarization is important for the stability of the voltage clamp circuit.

The technique for coating Ag wire was as follows. A piece of 0.008 inch diameter silver wire and a copper wire were connected to a 12V transformer adaptor, as shown in Figure 3.1. First, both wires were connected with the adaptor such that the silver wire acted as the cathode and copper as the anode. The wires were put into a small beaker with saturated NaCl solution for 15 seconds. This cleaned the surface of the Ag wire and made sure that no oxidized metals remained on the wire. Next, the polarity of the adaptor was reversed making the silver wire the anode and the copper wire the cathode. The wires were again placed into the NaCl solution to coat the Ag wire for approximately 3 minutes, or until the colour of the whole Ag wire had been changed to grey. The coated silver wire could be used as either a wire electrode or a conducting wire for a glass electrode.

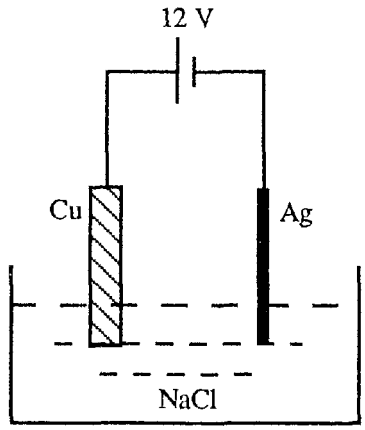

Figure 3.1 Set-up for coating silver wire A piece of 0.008 inch diameter silver wire and a copper wire were connected to a 12V adaptor. The two wires were then inserted into the sodium chloride solution in a Petri dish.

3.2.2 Glass pipette electrodes

A) Single glass filament electrode

A micropipette puller (MODEL P-87 FLAMING/BROWN MICROPIPETTE PULLER) was used to pull single glass pipettes. The outside and inside diameters of the

glass capillary tubing were 1.0mm and 0.75mm. The parameters of the puller were set as follows: Pressure (500), Heat (797), Pull (80), Velocity (70), and Time (200). After the electrode was pulled, the tip was broken to approximately 20 microns to lower its resistance. The electrode was then placed upside down into ACSF (tapering part of the glass was outside the solution), until the tip of the electrode was full of fluid. A needle was used to fill the base of the electrode.

B) Theta-tubing glass electrode

A similar method was used to make theta-tube glass electrodes. A theta-tube glass capillary has two channels separated by a glass plate. Two silver chloride coated silver wires were inserted into the two channels of a pipette, one of which was for current passing (I_p) and the other for voltage sensing (V_s). This structure was ideal for the I_p and V_s electrode wires which were expected to be very close to each other. After the theta-tubing glass was filled with ACSF, the top part of solution was removed at both openings of the theta-tube. This minimized the salt bridging effect which might short the I_p and V_s electrode compartments.

CHAPTER 4 EXPERIMENTAL EVALUATION OF THE VOLTAGE CLAMP TECHNIQUE

This chapter describes the evaluation of the voltage clamp circuit in ACSF. The effectiveness of wire and glass pipette electrodes are compared to each other and to the potential distribution predicted from basic principles in Chapter 2. The results of using a three-channel clamp circuit to generate voltage gradients in ACSF are also described.

4.1 Test of Voltage Clamp in ACSF

Since electrochemical phenomenon between the solution and the electrodes can produce unusual electronic properties, it is important to confirm that the voltage clamp circuit is stable in ACSF.

4.1.1 Testing the voltage clamp circuit in ACSF

Figure 4.1 shows a diagram of the circuit used to test the voltage clamp in ACSF. In this case wire electrodes were used. The current passing and voltage sensing wire electrodes were placed as close to each other as possible by glueing them together with epoxy resin. A ground return ring (Ag-AgCl wire) at the bottom of the dish carried current returning from the I_p electrode. Because of its connection to a high impedance amplifier, the V_s electrode did not carry any current. Thus it could sense the potential where the I_p electrode was located assuming the I_p and V_s wires were close enough to each other. Since a potential is always relative to a reference signal, a reference wire ring was also placed inside the solution. The circuit used a differential amplifier to measure V_s relative to this reference electrode. The rest of the circuit was similar to that described in Chapter 2 except for the addition of an offset correction integrator. When the switch was closed the

integrator nulled all the offsets in the feedback loop to zero. This was a necessary feature since glass and wire electrodes frequently have substantial and unpredictable offset voltages. An additional wire electrode (V_{pt}) was employed to generate a perturbing current in the solution in order to test if the circuit was still capable of voltage clamping.

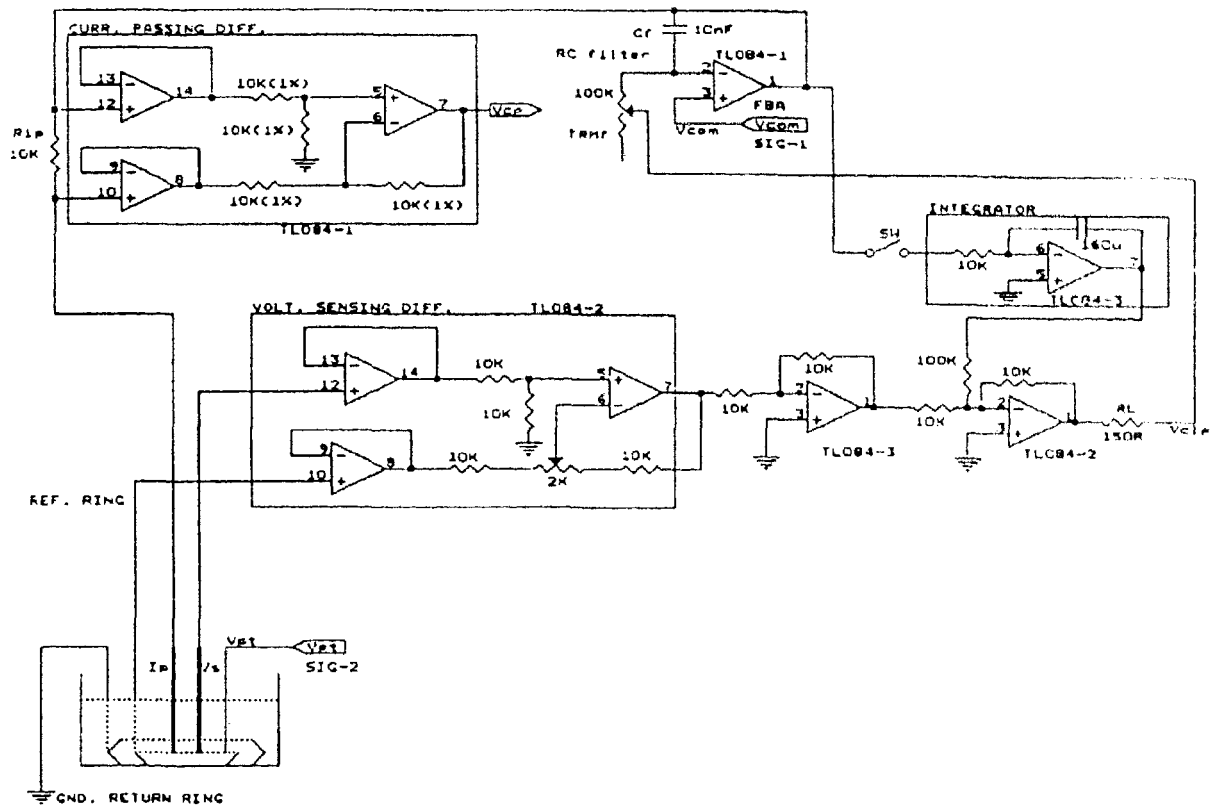

Figure 4.1 Voltage clamp circuit for testing in ACSF This extended voltage clamp circuit included: 1) a current passing differential amplifier (CURR. PASSING DIFF.) used to measure the amount of current (I_p) passing through the current passing electrode; 2) two wire electrodes I_p and V_s which were glued together as close as possible to each other; 3) a differential amplifier (VOLT. SENSING DIFF. BOX) to sense the voltage at the Vs electrode tip relative to the reference electrode (REF. RING); 4) an integrator (INTEGRATOR) to correct for offset and drift resulting from polarization at the interface between the electrodes and the solution.

4.1.2 Experimental protocol and results

Experiments with the circuit in Figure 4.1 were conducted in order to confirm that the circuit can voltage clamp the ACSF even during a perturbing signal. The first step of each experiment was to zero the DC offsets in the system. To do this, V_{com} was set to zero and the integrator switch was closed. After a few seconds the DC offsets were corrected and the switch was reopened. A series of command voltages were then applied to V_{com} and the V_{clp} was recorded for each step. Next a perturbing signal of 10mV was applied to the bath and the same series of commands were applied to V_{com}. This procedure was repeated using perturbing signals of increasing magnitude. Each set of data showed a close correspondence between the command and the resulting voltages as shown in Figure 4.2.

From graph (A) of Figure 4.2, the straight line with slope of one indicates that the clamp voltage (V_{clp}) was always equal to the command voltage (V_{com}) independently of the perturbing signal (V_{pert} was 40mV in the graph). This suggested that the clamp worked in the ACSF solution. A linear relationship between passing current I_p and command voltage V_{com} shown in Figure 4.2B also implied that the amount of current required was proportional to the clamped voltage V_{com}.

In conclusion, the voltage clamp circuit did work properly in ACSF solution even during a perturbing signal. The clamp circuit was then used to verify the theoretical potential predictions and to determine whether wire electrodes are indeed better at space clamping than micropipettes.

(A)

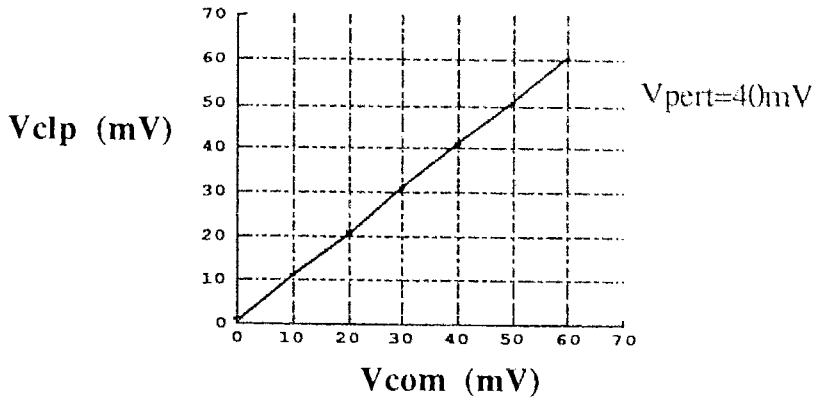

(B)

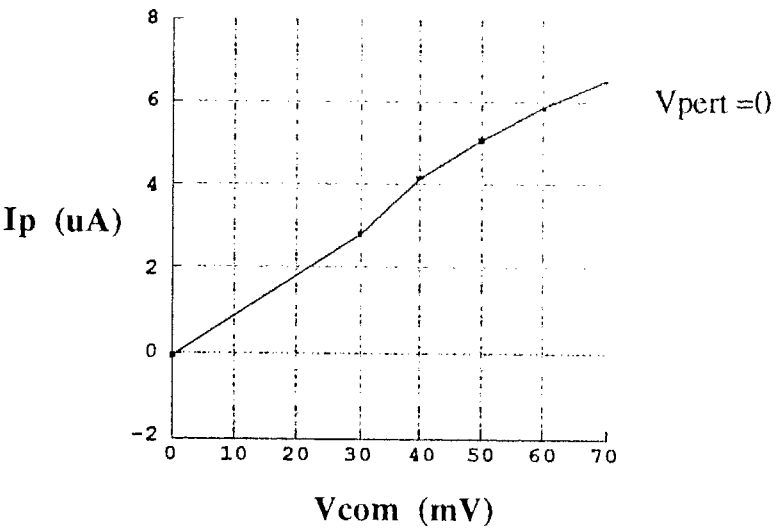

Figure 4.2 Results of the voltage clamp function test in ACSF Graph (A) shows the relationship between clamp voltage (V_{clp}) and command voltage (V_{com}) during a perturbing signal of 40mV. The straight line with slope of one indicates that V_{clp} is always following V_{com}, i.e., clamp is working properly. Graph (B) also shows a linear relationship between I_p and V_{com} at a zero perturbing signal, which implies that I_p is proportional to V_{com}.

4.2 Experimental Evaluation of the Theoretical Potential Distributions

Many differences exist between the ideal configurations discussed in Chapter 2 and the actual test system used to evaluate the voltage clamp circuit. For example, the spherical distributed ground for the point source was actually a ring of wire. One would expect that these differences would influence the characteristics of the potential distribution generated by the circuit. This is evaluated in the following sections which compare the actual and the theoretically predicted distributions.

4.2.1 Verification of a point current source field

A) Experimental set-up

The set-up for testing the potential distribution of a single point current source is shown in Figure 4.3. A two barrel micropipette made from theta-tubing was used to produce a point current source and to keep the current passing and voltage sensing electrodes very close to each other. A ring of silver chloride coated silver wire was placed around the periphery of a cylindrical dish for the current return of the I_p electrode. A similar ring of coated silver wire was used as a reference electrode. The dish was 12mm deep and 20mm in diameter. An additional electrode was used to probe the potential distribution generated in the ACSF field dish. High impedance followers HIF1 and HIF2 ensured that there was no current passing through the reference wire and the probing electrode. The "V-Clamp" box in the figure represented a voltage clamp circuit based on Figure 4.1. A multimeter at the output of differential amplifier 2 (Diff2) was used for measuring the potential from the probing electrode relative to the reference potential.

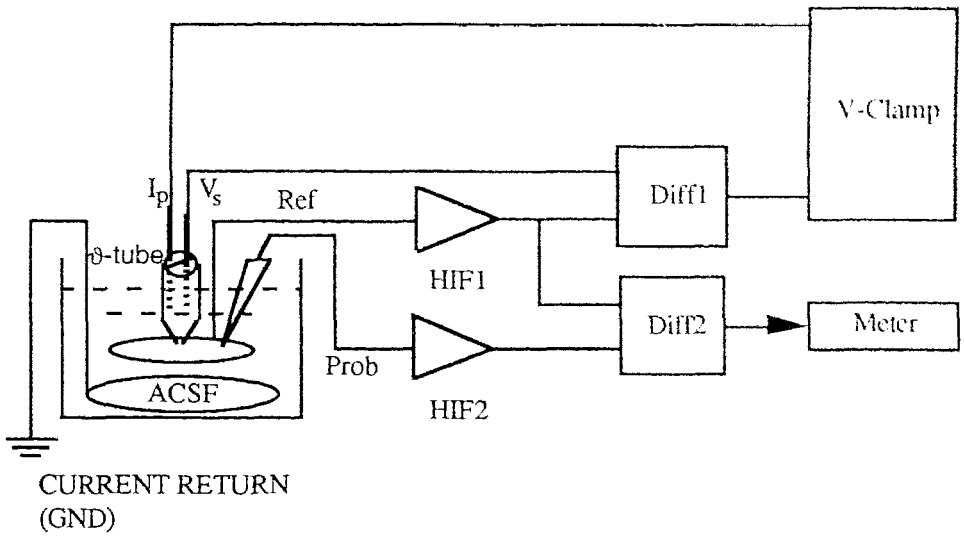

Figure 4.3 Set-up for verification of a single point source potential profile This was the set-up for testing a single point source field potential. Theta-tubing glass was used to produce a two barrel clamping electrode. This approach guaranteed that the current passing and voltage sensing electrodes were very close to each other. A ground wire ring (Ag-AgCl) was placed around the periphery of an ACSF filled dish for the current return of I_p. A reference electrode (Ag-AgCl wire ring) acted as a potential reference inside the solution. The probing electrode was employed to record the potentials at different locations inside the solution. Finally, high impedance followers HIF1 and HIF2 ensured that there was no current passing through the reference wire and the probing electrode. The "V-Clamp" box in the figure represented a voltage clamp circuit based on Figure 4.2. A multimeter at the output of differential amplifier 2 (Diff2) was for measuring the potential from the probing electrode relative to the reference potential.

B) Recording protocol and results

The measurement protocol was: 1) null offsets within the circuit by activating the offset correction integrator (refer to Figure 4.1). That is, make the output of the voltage sensing differential amplifier (Diff1) zero when V_{com} is zero. 2) move the probing electrode to different locations inside the solution, while recording the output of the differential amplifier 2 under the conditions of V_{com}=0 and V_{com}=constant. The difference between these voltages (V_{com1}-V_{com0}) gives the potential generated by the clamp at a specific location. The distance from the clamping electrode to the recording location was also measured.

Thirteen complete sets of data were recorded. A statistical package, SYSTAT, was used to analyse and plot these data. Curve fitting was carried out to see how the data fit the theoretical predictions of the point source field and the wire source field by calculating their residuals and corrected correlation coefficients (Table 4.1). In the table, S_{res} is sum of squared residual, and R_c^2 is corrected squared correlation coefficient. Nine out of thirteen sets of data suggested that the data supported the theoretical prediction of point source field ($\Phi=K_1+K_2 \cdot 1/r$) very well with grater than 0.9 of squared correlation coefficient. The results were also compared to the theoretical prediction for a wire current source ($\Phi=K_1+K_2 \cdot \ln 1/r$). When the residuals and correlation coefficients for the point and wire source were compared, nine of 13 data sets fit the point source better than the wire source predictions.

DATA SET	POINT FIELD	FITTING	WIRE FIELD	FITTING
	S_{res}	R_c^2	S_{res}	R_c^2
1	0.018	0.994	0.233	0.919
2	0.580	0.979	1.870	0.933
3	0.460	0.980	4.569	0.803
4	0.444	0.974	3.639	0.784
5	0.049	0.976	0.098	0.952
6	0.029	0.980	0.085	0.942
7	0.033	0.994	0.455	0.919
8	0.365	0.982	0.784	0.961
9	0.068	0.997	2.073	0.923
10	3.298	0.882	3.285	0.882
11	0.628	0.938	0.095	0.991
12	7.247	0.887	1.085	0.983
13	1.695	0.878	0.423	0.970

Table 4.1 Analysis of point source field These data were recorded using the single point source set-up shown in Figure 4.3. Using the program SYSTAT, residuals and correlation coefficients were calculated for both point and wire field predictions. S_{res} is sum of squared residual, and R_c^2 is corrected squared correlation coefficient.

The predicted and observed data were also compared graphically. All data sets were averaged and plotted as shown in Figure 4.4. The curve decayed quickly towards zero as the probing electrode was shifted away from the tip of the clamping electrode. A

comparison of the mean curve to the curves predicted on theoretical grounds for a point and a wire source is shown in Figure 4.5. Visually, the mean curve (white squares) fits the predicted curve for a point source (black circles) better than for a wire source (black squares). This impression was confirmed by comparing the residuals of both curve fittings at each location. These residuals were generated by taking the absolute value of the differences between the experimental result and the predicted value for each of the 13 data sets. The average and standard error of these values are shown in Figure 4.6. For all but the 3 most distant points, the average of residuals was less for the point than the wire source predictions.

In conclusion, the data from the single point current source experiment fit the theoretical prediction very well. Although these data fit a point source better than a wire source in most cases, four of 13 data sets had the opposite relationship. This variability is not surprising considering the differences between the theoretical assumptions and the actual recording conditions. For example, a ground ring was used instead of a sphere. Furthermore, various subtle differences between the set up in each experiment are likely to have occurred. For example, the exact location of the ground and reference rings or the depth of the ACSF may have differed.

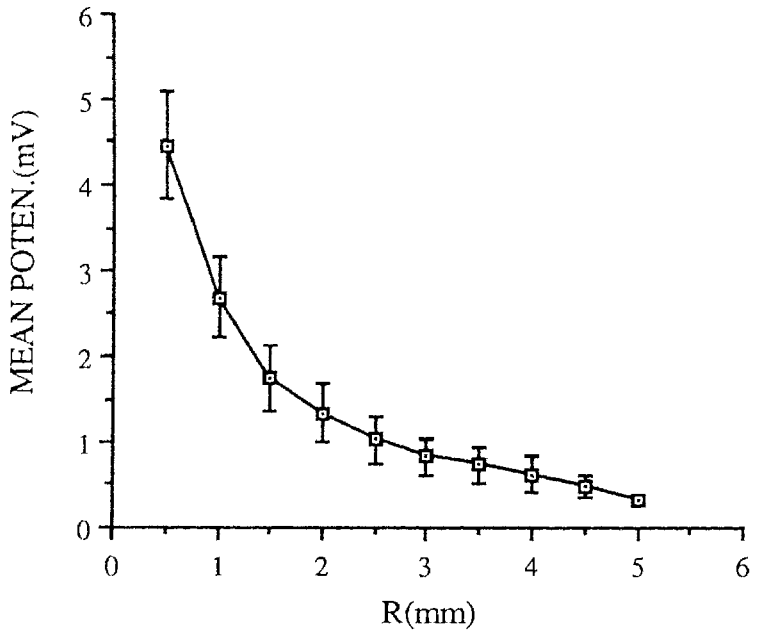

Figure 4.4 Mean potentials of the point source data The figure shows the average of the 13 data sets in Table 4.1. Each point is the average potential (±SE, Standard Error) at a specific distance (R) from clamping electrode. The curve decayed rapidly from the point source towards the ground.

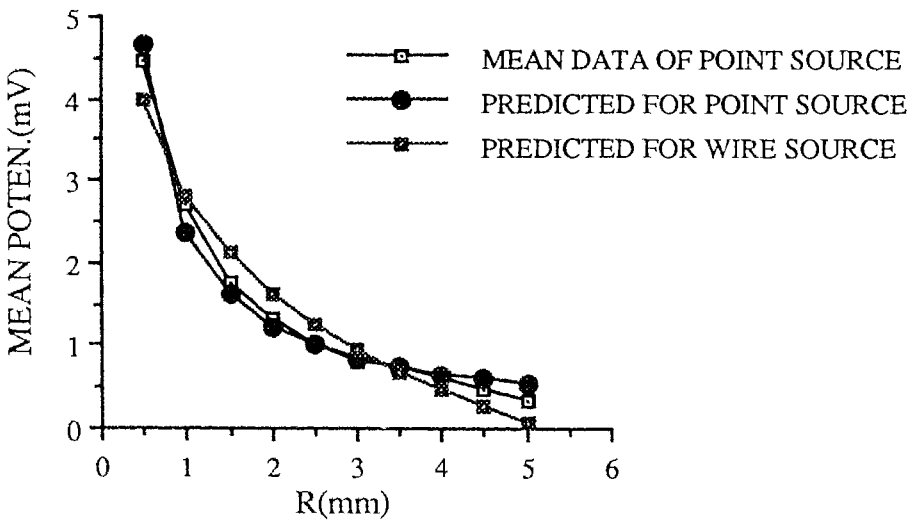

Figure 4.5 Mean point source data with predicted curves The averaged point source curve of Figure 4.6 is shown (white squares) superimposed on the theoretical curves for a wire (black squares) and point (black circles) source. Note that the mean curve closely follows the curve predicted for a point source.

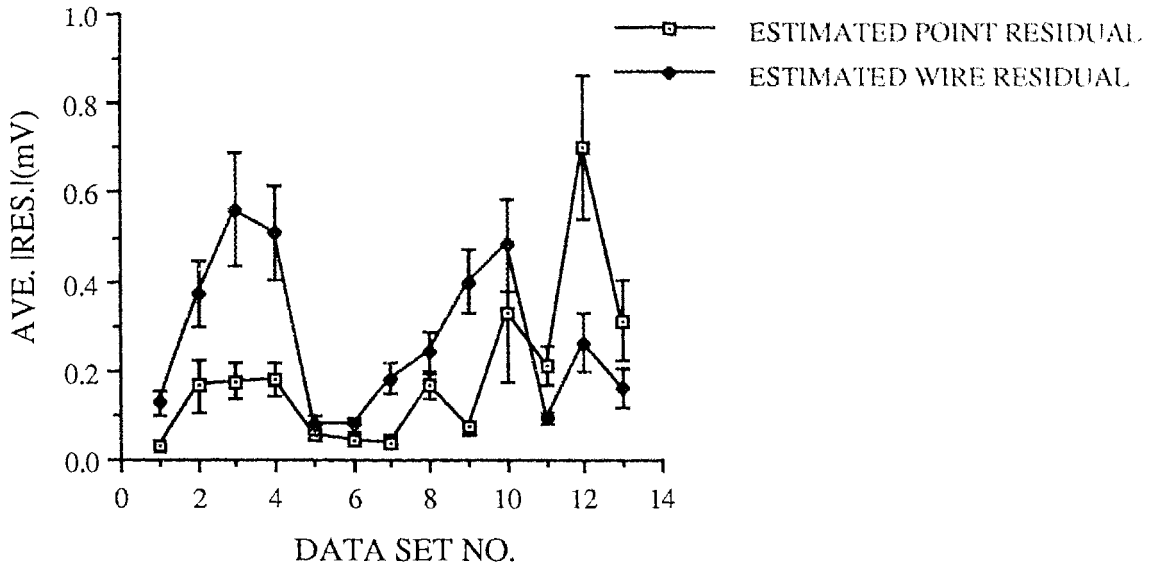

Figure 4.6 Average absolute residuals of point source data This figure shows the mean absolute residuals (±SE) for both point and wire source curves when compared to the 13 data sets.

4.2.2 Verification of a wire source field

A) Experimental set-up

The set-up for testing a single wire field potential distribution shown in Figure 4.7 was exactly the same as that for testing the point source field, except that wire electrodes were used instead of a two barrel micropipette. By glueing two silver chloride coated silver wires together with epoxy resin, current passing (I_P) and voltage sensing (V_S) wires were kept within 500 microns of each other.

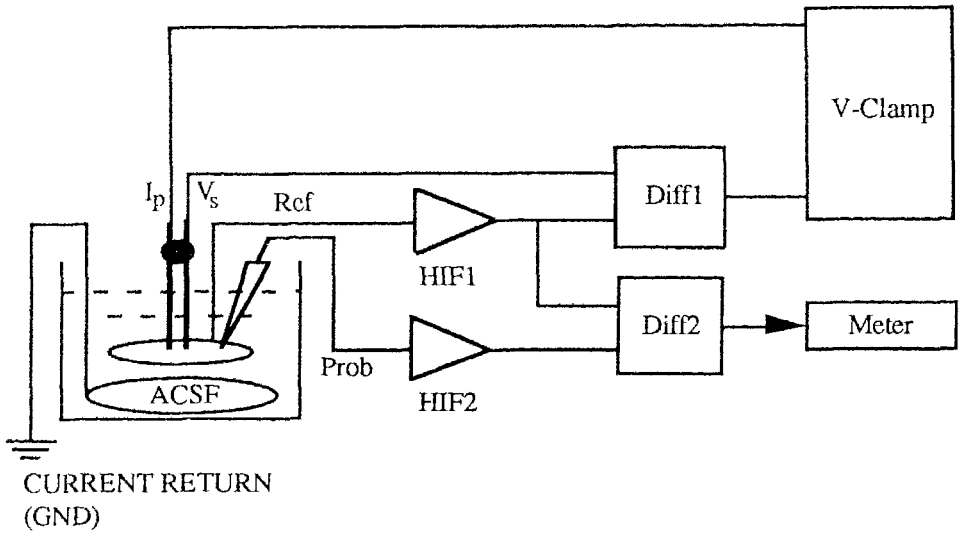

Figure 4.7 Set-up for verification of a single wire source potential profile
The set-up for testing the single wire source field was similar to the experimental set-up for a single point field (Figure 4.3), except that wire electrodes (I_p and V_s) replaced the theta-tubing electrode.

B) Recording protocol and results

The recording protocol was the same as for the point source experiment described previously. Ten sets of data were recorded. Curve fitting results are shown in Table 4.2. Seven out of ten had correlation coefficients greater than 0.8 when compared to the curve predicted for a wire source and all but one fit the curve for a wire source better than that for a point source.

DATA SET	WIRE FIELD	FITTING	POINT FIELD	FITTING
	S_{res}	R_c^2	S_{res}	R_c^2
1	0.229	0.914	0.634	0.762
2	4.608	0.835	9.100	0.674
3	0.353	0.800	0.651	0.632
4	0.704	0.973	2.393	0.909
5	0.821	0.984	4.133	0.919
6	1.260	0.926	3.968	0.767
7	1.969	0.890	4.948	0.723
8	3.093	0.584	4.950	0.334
9	1.553	0.499	2.460	0.207
10	2.200	0.905	1.418	0.939

Table 4.2 Analysis of wire source field These data were recorded using the set-up shown in Figure 4.7. Using the program, SYSTAT, residuals and corrected correlation coefficients were calculated for both point and wire field predictions. S_{res} is sum of squared residuals and R_c^2 is the corrected squared correlation coefficient.

The predicted and observed data were also compared graphically. The mean voltage profile for 10 data sets is shown in Figure 4.8. The voltage slowly decayed from a peak value near the current source to zero near the ground return wire. The same curve is shown superimposed on the predicted curve for a wire and point source in Figure 4.9. Visually these results (white squares) fit the predicted curve for a wire source (black circles) better than that for a point source (black squares). This impression was confirmed by comparing the residuals of both fittings at each location in the same manner described in the previous section for the point source results. As seen in Figure 4.10, for all but the last point the average of the residuals was less for the wire source than the point source predictions. The results obtained with a wire electrode were also compared to the point source results obtained previously. The mean curves for both data sets are normalized and superimposed in Figure 4.11. Note that the wire source curve has a more gradual decay than the point source.

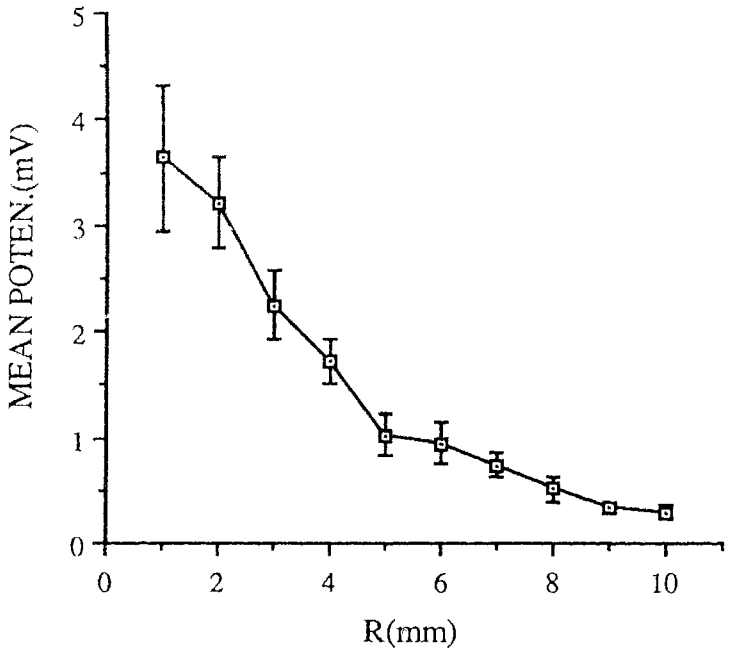

Figure 4.8 Mean potentials of the wire source data The graph shows the average of the 10 data sets in Table 4.2. Each point is the average potential (±SE) at a specific distance (R) from the clamp electrode.

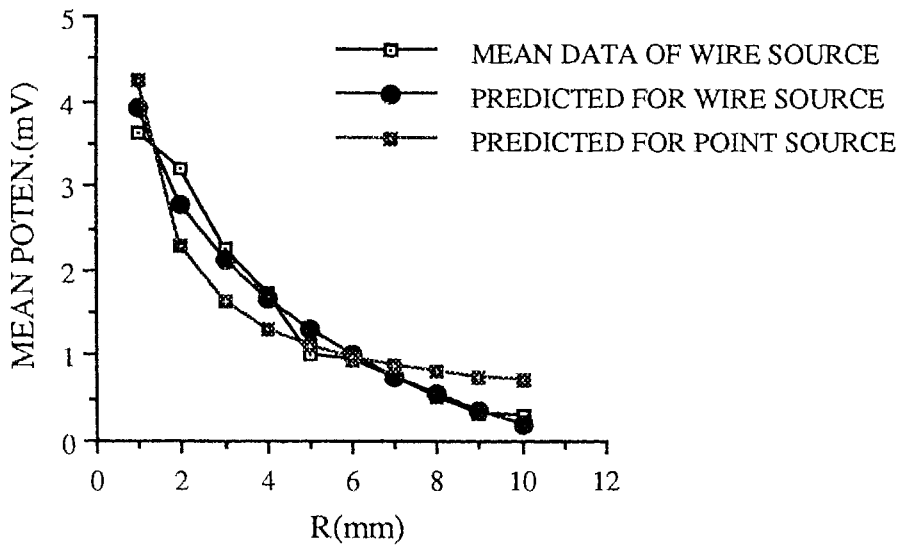

Figure 4.9 Mean wire source data with predicted curves The averaged wire source curve of Figure 4.8 is shown (white squares) superimposed on the theoretical curves for a wire (black circles) and point (black squares) source. Note that the mean curve closely follows the curve predicted for a wire source.

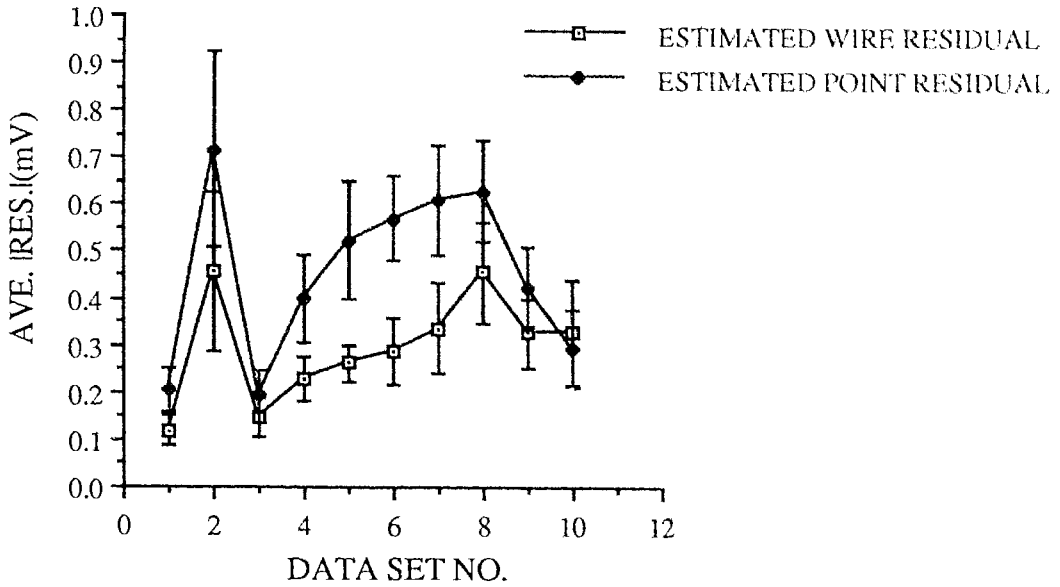

Figure 4.10 Average absolute residuals of wire source data This figure shows the mean absolute residuals (±SE) for both wire and point source predicted curves when compared to the 10 sets of data.

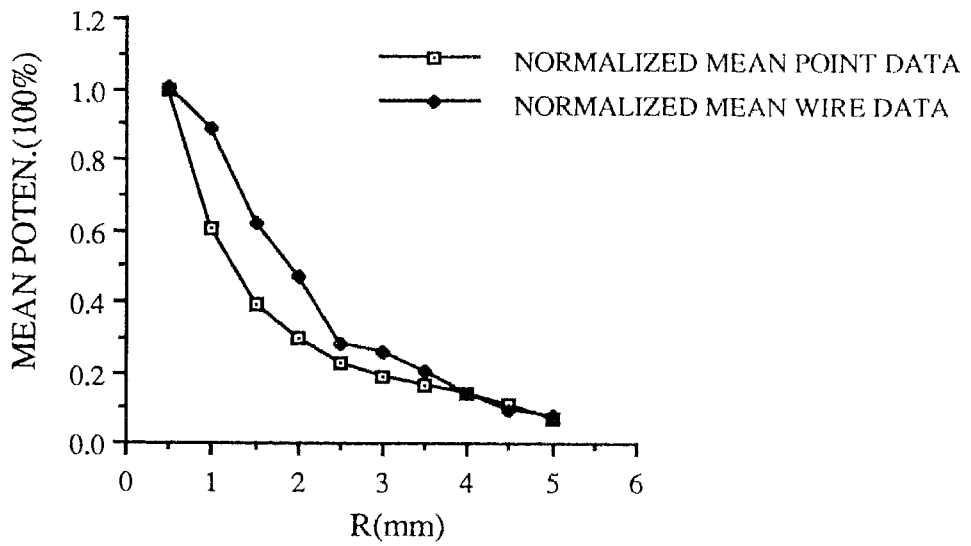

Figure 4.11 Normalized mean potentials of the point and wire source data The mean potential curves for point and wire current sources taken from Figure 4.4 and 4.8 are normalized. More gradual voltage decay is seen for the wire source (black diamonds).

4.2.3 Summary

Recordings using point and wire current sources revealed that ACSF field potential distributions generated by the voltage clamp circuit are similar to those predicted theoretically. The differences are likely to be related to the various physical differences between the theoretical and actual set-up. The results also confirm that a wire source electrode should be more effective at clamping the ACSF than a point source electrode.

4.3 Generation of a Voltage Gradient in ACSF

To produce a voltage gradient in a solution, at least two channels of voltage clamp are required. This section describes the results obtained using a two-channel and a three-channel voltage clamp circuit. The multi-channel system was first tested on the bench to confirm that the circuit was stable. The multi-channel system was then tested in ACSF using wire electrodes.

4.3.1 Two-channel voltage clamp system

A) Experimental set-up

The experimental set-up for generating a voltage gradient in a two-channel system is shown in Figure 4.12. Two voltage clamp circuits ("V-Clamp1&2" in the figure) were exactly the same as the single channel circuit discussed in the previous sections. A voltage gradient was generated by setting a relatively high V_{com1} and low V_{com2}. Under these conditions, the I_{p1} electrode would function as a current source and the I_{p2} electrode as a current sink (note the directions of arrows in Figure 4.12). No current return (ground) wire ring was required in the solution, since the current could go from the first channel I_{p1} wire, through the solution and back to the second channel I_{p2} wire. Thus the current could only flow between the two electrode tips. Furthermore, the two voltage sensing wires (V_s) were

the reference electrode for each other, so there was no need for a reference electrode ring inside the solution. The ACSF was 8mm deep in a dish, and the wires were immersed to a depth of 0.5mm. The distance between the electrode assemblies was 4mm.

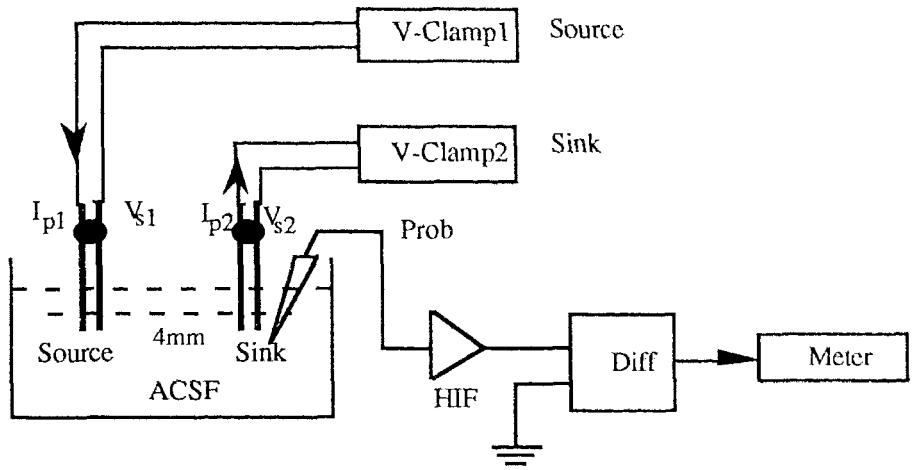

Figure 4.12 Two-channel voltage clamp system This was the experimental set-up for generating a voltage gradient in a two-channel system. I_{p1}, I_{p2} wires acted as a current source and sink, thus no current return (ground) wire ring was required. Also, the voltage sensing wires were the reference electrode for each other. The two V-Clamp circuits were exactly the same as the single wire source set-up shown in Figure 4.9. The solution was 8mm deep, and the wires were immersed to a depth of 0.5mm. The distance between the two electrode assemblies was 4mm.

B) Recording protocol and results

Voltage recordings were obtained from a 2 dimensional grid of points in a plane parallel to the ACSF surface with one axis of the plane parallel to the line joining the two electrode assemblies. Measurements were made at 0.5mm intervals at a depth of 0.5mm. Figure 4.13 shows the mean of five sets of recorded potentials. Plot (A) shows that an approximately linear potential distribution was present between the electrode assemblies. The maximum and minimum potential occurred at the locations of the clamp electrodes (dashed lines) and decayed in all directions. Plot (B) shows a contour graph of the entire two dimensional array of recording locations. The isopotential lines of the plot are similar

to those expected for a simple dipole. The plots suggested that an approximately linear potential distribution could be generated by a two-channel voltage clamp system with wire source electrodes.

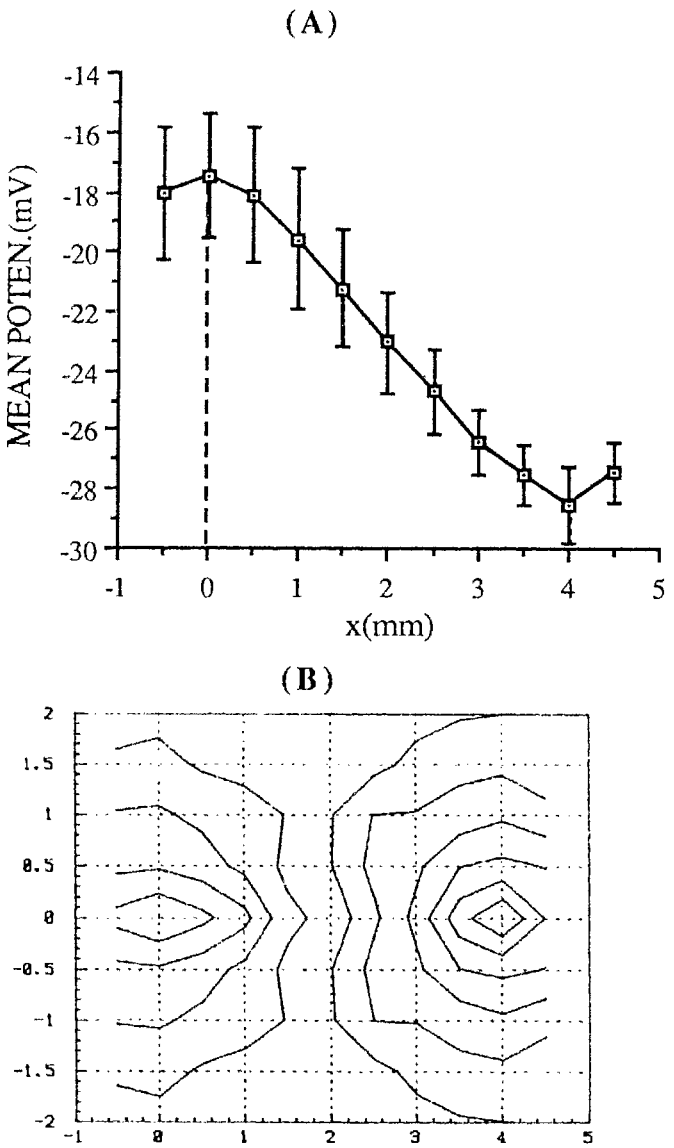

Figure 4.13 Mean potential distribution using a two-channel voltage clamp Plot (A) shows the averaged voltage (±SE) recorded at each location along the line joining the two electrode assemblies. A contour plot of the entire array of voltage recording is shown in plot (B). Each line represents an isopotential region.

4.3.2 Three-channel voltage clamp system

A useful extracellular voltage clamp will require several clamping points distributed throughout the volume. In the simplest case a linear array of clamping locations will be required. This section evaluates the properties of a linear array of clamping points using a three-channel circuit. The experimental set-up for a three-channel clamp system is shown in Figure 4.14. It was basically the same as that for the two-channel system (Figure 4.12) with the addition of a third channel. The distance between each clamp location was 3mm.

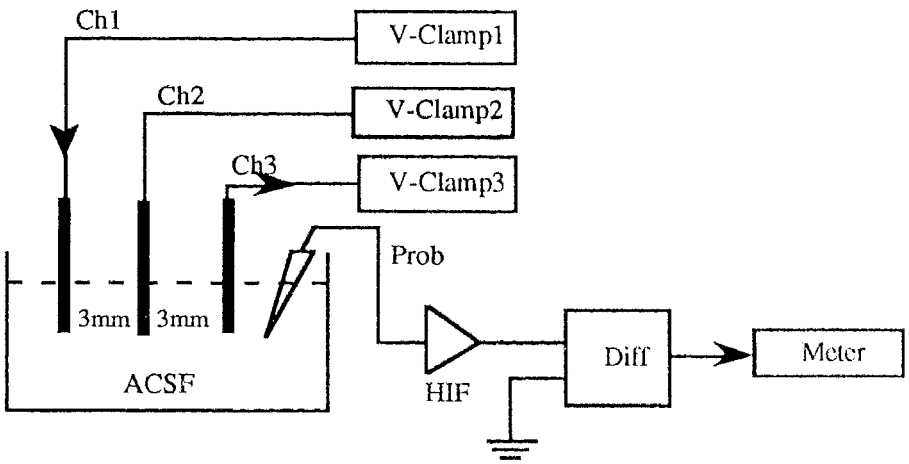

Figure 4.14 Three-channel voltage clamp system This figure shows a three-channel voltage clamp system with three electrode assemblies. Each channel had exactly the same configuration as the single-channel system (Figure 4.7). The probing electrode recorded the potential at a series of points along the line joining the electrode assemblies.

With three channels it was possible to generate more complicated extracellular potentials. In the example presented in this section, the three channels were set to clamp at 20mV, 0mV and -5mV. As in the previous section, ground and reference electrodes were unnecessary since these functions are served by the extra channel in the system. The mean voltage profile of these complete data sets is shown in Figure 4.15. The circuit successfully clamped the potential at the locations of the electrode assemblies with a gradual shift in potential between these sites.

In conclusion, the three-channel voltage clamp system was also stable in the ACSF solution, and a voltage gradient could be generated by setting the command voltages at positive, zero and negative values.

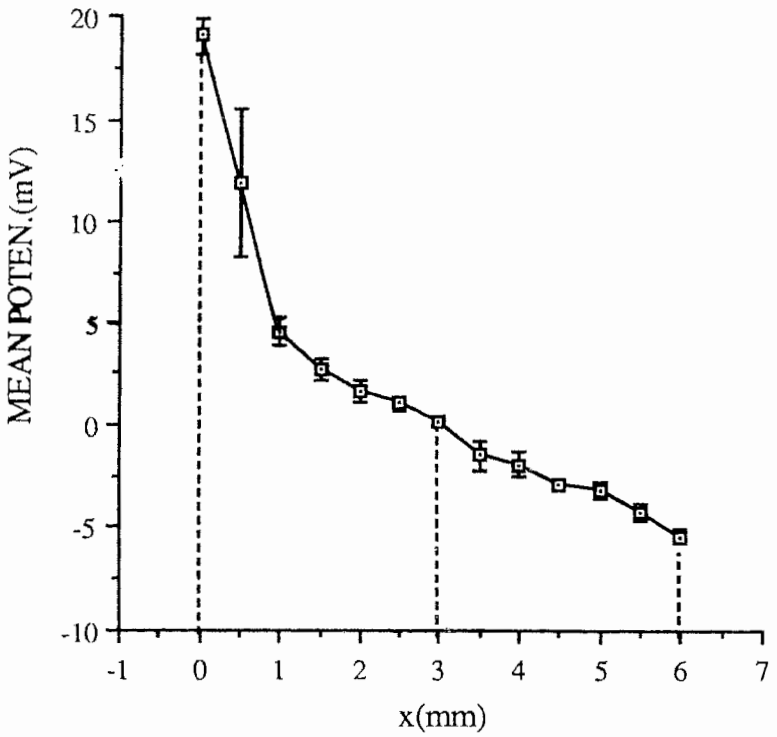

Figure 4.15 Mean potential distribution using three-channel voltage clamp This curve shows a voltage profile (±SE) of the mean potential distribution from 3 sets of measurement. The command voltages were 20mV (V_{com1}), 0mV (V_{com2}) and -5mV (V_{com3}). The three electrodes were located at 0, 3 and 6mm as specified by dashed lines.

4.3.3 The effect of a perturbing signal on the voltage clamp

A useful voltage clamp device must be capable of clamping the extracellular space even during transient physiological signals. This section evaluates the three-channel voltage clamp system in ACSF during artificially generated perturbing currents.

A) Voltage clamp test during perturbation

(a) Experimental set-up

The set-up for evaluating the three-channel voltage clamp system with a perturbing signal is shown in Figure 4.16. Two silver chlorided perturbing wires were connected to a 9V battery and a 100KΩ trimpot. When the switch K1 was closed, a current passed between the wires resulting in perturbation of the voltage throughout the ACSF. Switch K2 was used to disconnect channel 1 and 3 and therefore disable the voltage clamp. There was no switch on the second channel since it functioned as a voltage reference for the probing electrode when the clamp was off. The probing electrode was used to record the potential along the line joining the three electrode assemblies.

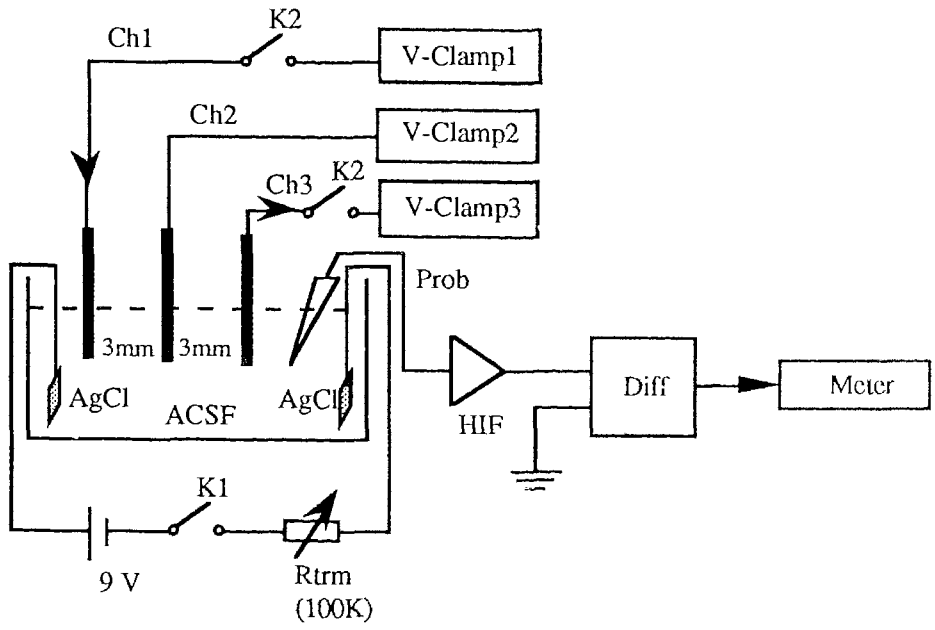

Figure 4.16 Three channel system with perturbation This was the set-up for a three-channel voltage clamp circuit with a perturbing signal. Two silver chlorided perturbing wires were connected to a 9V battery and a 100KΩ trimpot. K1 was a switch for controlling the perturbing signal. Switch K2 was used at the feedback loop of each clamp circuit to control the presence of the clamp function in each channel. There was no switch at the feedback loop of the second channel.

(b) Recording protocol and results

Command voltages were set at 15mV (V_{com1}), 0mV (V_{com2}), 15mV (V_{com3}). The recordings were carried out under four different conditions: (1) Voltage clamp off and no perturbing signal (K2 and K1 open); (2) Voltage clamp on and no perturbing signal (K2 close, K1 open); (3) Voltage clamp off and perturbing signal present (K2 open, K1 closed); (4) Voltage clamp on and perturbing signal present (K2 and K1 closed). The probe electrode was used to measure the voltage at each point under all four conditions. The results of 3 experiments are plotted on separate graphs in Figure 4.17. The paradigm for the three experiments differed only in the location of the perturbing signal.

In each case, the voltage was successfully clamped without (black diamonds) or with (white triangles) the presence of a perturbing signal (white circles) at the clamping electrodes. However, the potential at the points between the clamping electrodes were affected by the perturbing signal (shown by white triangles). This influence was larger midway between the clamped locations. In the figure, black squares indicate the sum of the clamped signals without perturbation and the perturbing signal alone. The similarity of these points to the intermediate values recorded under the clamped (black diamonds) and perturbed (white circles) conditions suggests that the perturbing signal can still influence the potential between the clamped locations.

(c) Conclusions

The results in Figure 4.17 confirm that the three electrode clamp is stable and is capable of clamping the potential near the clamping electrodes even in the presence of a perturbing signal. However, the clamp is less effective at canceling the perturbing currents at intermediate locations between the clamping electrodes.

(A)

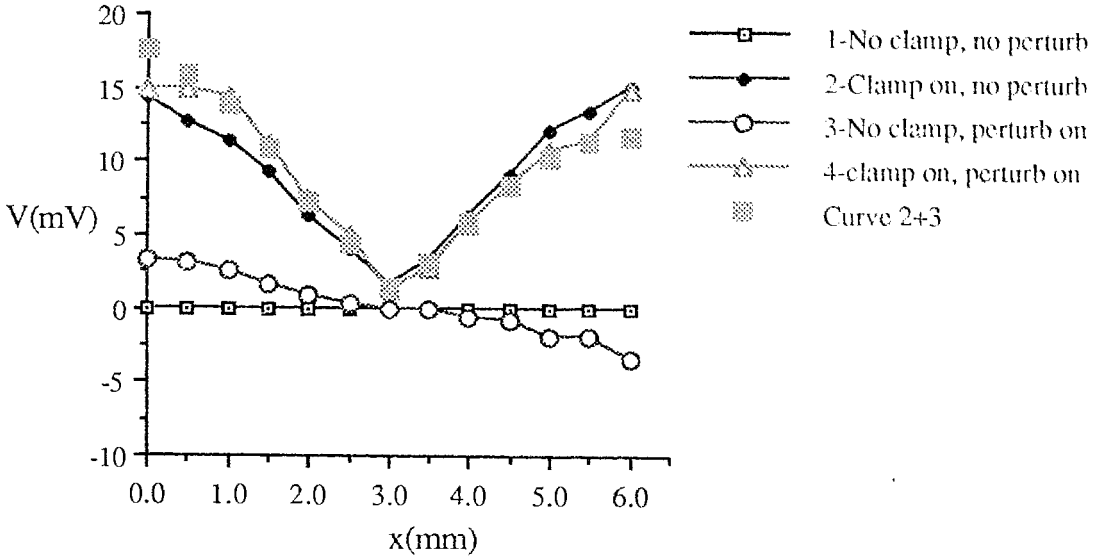
20
15
10
V(mV) 5
0
-5
-10
0.0 1.0 2.0 3.0 4.0 5.0 6.0
x(mm)
1-No clamp, no perturb
2-Clamp on, no perturb
3-No clamp, perturb on
4-clamp on, perturb on
Curve 2+3

(B)

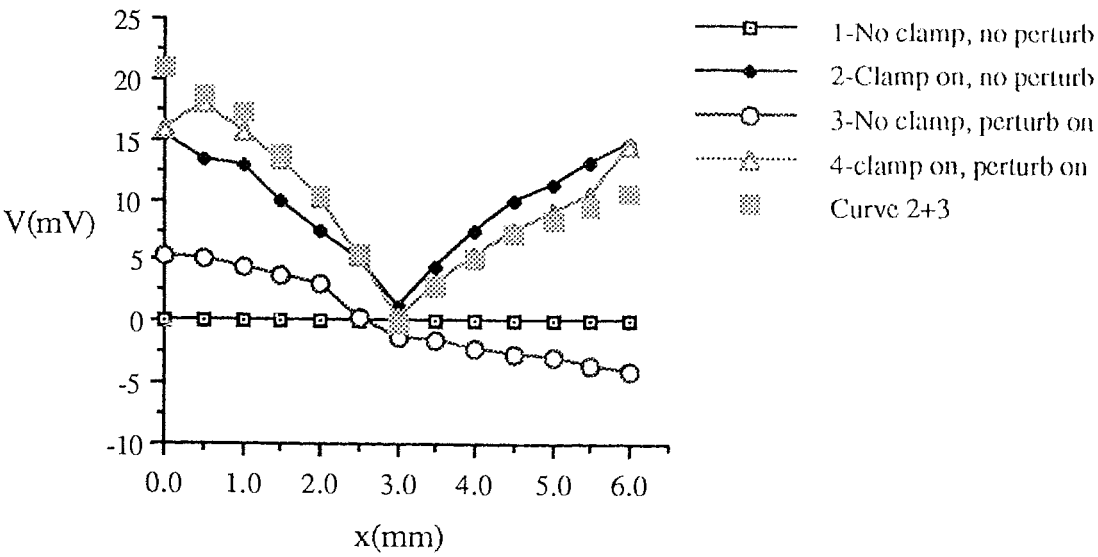
25
20
15
10
V(mV) 5
0
-5
-10
0.0 1.0 2.0 3.0 4.0 5.0 6.0
x(mm)
1-No clamp, no perturb
2-Clamp on, no perturb
3-No clamp, perturb on
4-clamp on, perturb on
Curve 2+3

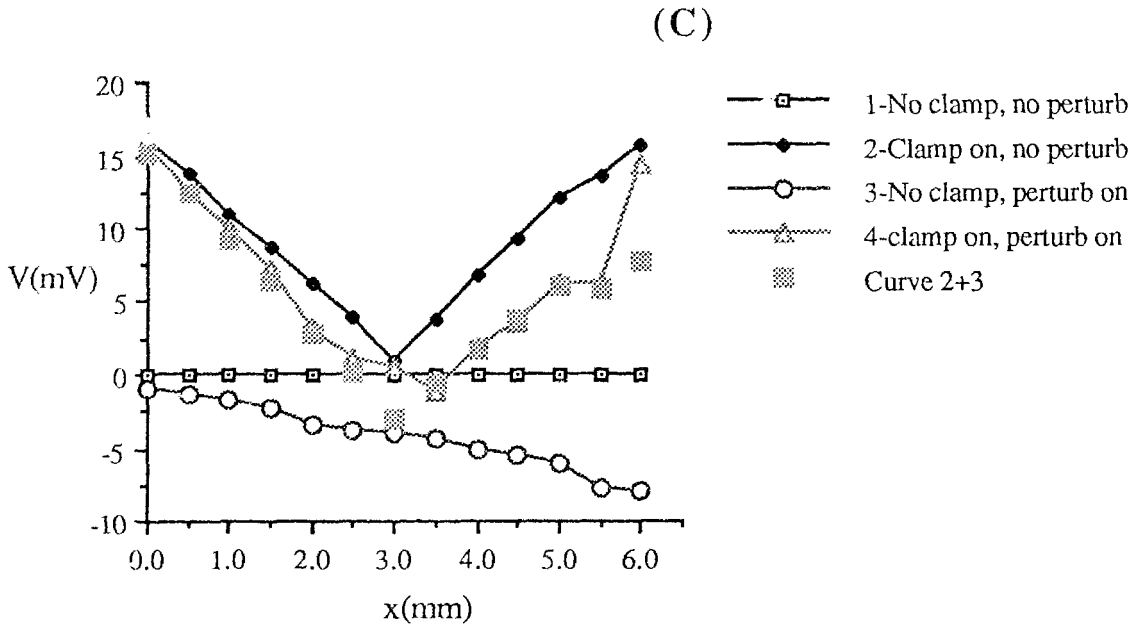

Figure 4.17 Results using the three-channel system with perturbation Command voltages were set at 15mV(V_{com1}), 0mV(V_{com2}), and 15mV(V_{com3}). Recording of the potentials was taken under four different conditions which are indicated by four different symbol curves in the figure: (1) Voltage clamp off and no perturbing signal (K2 and K1 open); (2) Voltage clamp on and no perturbing signal (K2 close, K1 open); (3) Voltage clamp off and perturbing signal present (K2 open, K1 closed); (4) Voltage clamp on and perturbing signal present (K2 and K1 closed). The probe electrode was used to measure the voltage at each point under all four conditions. The results of 3 experiments are plotted on separate graphs in the figure. The paradigm for the three experiments differed only in the location of the perturbing signal.

B) Measurement of the clamping current (I_p)

The voltage clamp system also needs to be evaluated in terms of its basic working principles. That is, to measure how much current is required to pass through the electrodes in order to maintain a desired voltage. This will help give an insight into the relationship between current generated by the perturbation and the clamping function.

(a) Measurement set-up

The same experimental set-up was used as shown in Figure 4.16 except that the current passed by the electrode I_p was also measured. By changing the perturbing current I_{pert}, the relationship between I_p and I_{pert} was investigated.

(b) Recording protocol and results

During each measurement, command voltages were 20mV, 0 and -20mV for the first, second and third channel, such that the first channel was always a current source, and the third channel was a current sink. The perturbing current I_{pert} was changed from high to low by varying the trimpot resistance on the battery leads, as shown in Figure 4.16. The results are shown in Figure 4.18. The bar chart indicates that the voltage clamp channels increased their current output in order to clamp the larger perturbing signal.

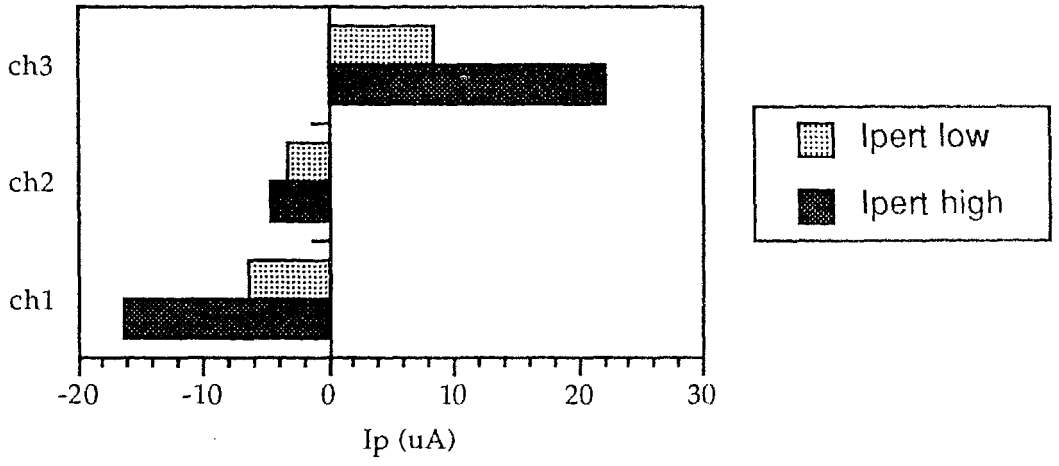

Figure 4.18 Relationship between I_p and I_{pert} This bar graph shows the clamp current, I_p, for three channels under different magnitudes of perturbing current, I_{pert}. The passing current, I_p, was larger when the perturbing current, I_{pert}, was larger.

(c) Conclusion

The results of the measurement in Figure 4.18 indicate that the voltage clamp circuit was indeed varying the current I_p to compensate for the perturbation applied to the solution. The more perturbation, the more current was used to maintain the clamped voltages.

CHAPTER 5 DISCUSSION AND CONCLUSIONS

5.1 Discussion

Some theoretical and practical problems involved in the development and evaluation of the voltage clamp technique were considered and overcome to stabilize the clamp system in ACSF solution. This is discussed in the following section.

5.1.1 Theoretical estimation of potential distribution

The theoretical potential distributions for the point and wire current source field indicated that the voltage decays slower in a wire source field than in a point source field.This is correct only if the same initial boundary conditions exist. The location and configuration of the ground set-up also affect the potential profile. The theoretical curves were based on the assumption that the ground around a point current source is a sphere allowing current to spread in 3 dimensions, and that the ground around a wire current source is a cylinder allowing current to spread in 2 dimensions.

5.1.2 Circuit stability

During the development of the voltage clamp circuit, 60Hz noise coming from the power supply became a significant factor. To minimize the AC noise level, shielded wires and a metal box were used to mask electromagnetic noise. Grounding all the equipment used for making measurements also lowered the noise. DC offset and drift generated at the electrode-solution interface required the addition of an offset correction integrator to the basic circuit.

During the phase of experimental testing of the circuit in ACSF, silver chloride coated silver wire had to be used to decrease the polarization of the electrode at the interface between the electrode and the solution. Electrode polarization was also minimized by limiting the magnitude and duration of current passing through the electrode. Salt bridging across the theta-tubing was another problem which produced difficulties during data collection. It occurred when the two wires inserted into the channels of the theta-tubing were shorted together via a bridge of dried ACSF. Therefore current could pass directly between the voltage sensing and the current passing wire instead of going through the solution. Clearly, this would cause the clamp to fail. Using a needle to remove part of electrode conducting solution at the top of theta-tube reduced the salt bridging problem.

5.1.3 Error analysis of experiment results

Some specific technical and operational errors involved in the experiments may be responsible for deviation of the results from the theoretical expectations. First of all, none of the point and wire source experimental set-ups for potential measurement completely matched the theoretical conditions. The ground in the point source was not a sphere, and the ground in the wire source was not a cylinder. In both cases a wire ring was used. Secondly electrodes for passing current had a finite length, less than the depth of the ACSF. These differences could bring about differences between the theoretical and observed curves for both point and wire source models.

Operational errors could also account for variability in the results. These include inaccurate location of the probing electrode as well as variations in the precise location of the reference wire ring and the current passing electrodes.

In general, variability in the experimental results could be improved by the finer control of measurement and experimental conditions.

5.2 Conclusions

(1) The theoretical predictions for field potential distributions indicate that a wire electrode should be better than a micropipette since the field potential for a wire current source decays more slowly. The results also suggest that the cable characteristics for a short silver chloride coated silver wire in ACSF can be ignored since its electrotonic length λ is very large. Wire electrodes are, therefore, an appropriate current source for future voltage clamp experiments.

(2) Analyses of the data from experiments in ACSF match the theoretical predictions for field potential distributions in point current source and wire current source fields very well. The results of curve fitting to the predicted field potentials indicate that point and wire source fields are not significantly different although they do tend to have a better fit to the corresponding predicted profile.

(3) A stable and approximately linear potential distribution, or voltage gradient, can be generated in ACSF by a three-channel voltage clamp system with no ground return wire inside the solution.

(4) Upon the presence of a perturbing current in the ACSF the locations at the voltage clamp electrodes in the solution can still be clamped, but the potential profile between the electrodes is distorted. That is, the voltage clamp circuit only completely clamps the tips of voltage clamp electrodes.

Successful development of a technique capable of generating a voltage gradient in ACSF may prove to be an effective method to investigate the possible role of ephaptic interactions in epileptic seizures. This study confirmed our original hypothesis that voltages in a volume of electrolyte, not unlike the extracellular space in the brain, can be controlled artificially by a multi-channel voltage clamp system. The success of this project is a first step towards the development of an important tool for brain research involving the study of extracellular field potentials.

CHAPTER 6 APPENDIX

Potential Distribution of a Single Wire Source Field

Consider a finite cable, as shown in Figure 6.1(A), through which the current is passing. The initial potential and current in the wire are V_o and I_o, respectively. As current passes through the wire, the amount of current decreases in both longitudinal and radial axis because of leakage current through the wall (i_w) and the voltage drop along the wire, i.e., the leakage current through the wire wall i_w and the axial current i_a becomes less along the length of the wire from its initial segment. The cable can be modeled an electrically equivalent circuit within a conductor medium, as shown in graph (B). r_a is a resistor of each small segment along the cable axial direction, r_{cw} and r_m are the cable wall resistor and medium of that segment. At a certain distance g, the axial and the wall current are assumed to be i_{ag} and i_{wg}, and the voltage is V(g). Ground (GND) is set at a finite place (r_{gn} is the distance of the ground from the center of the wire) in the external medium.

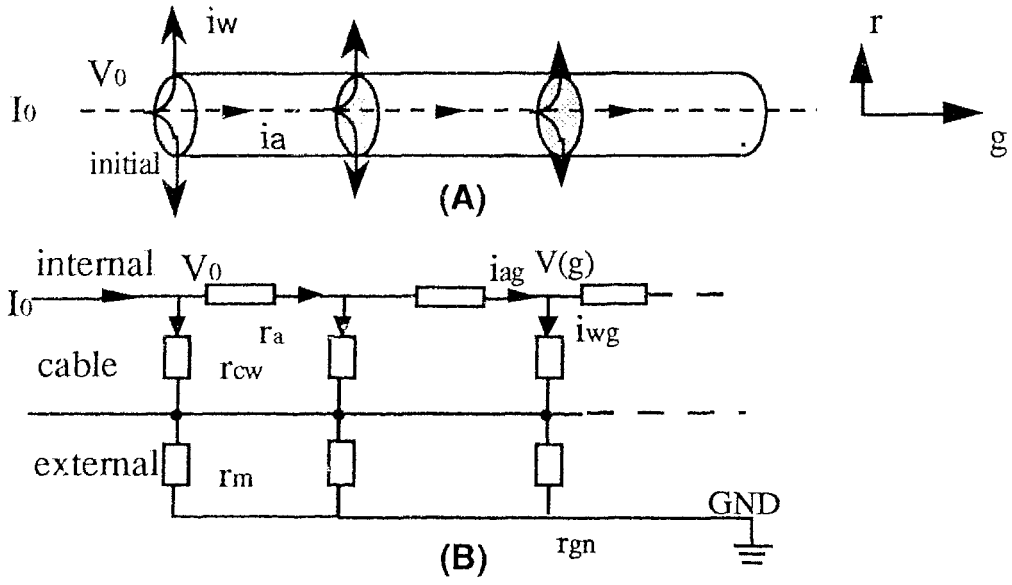

Figure 6.1 A single wire source and its electrically equivalent circuit The graph (A) shows a finite cable through which current is passing. The potential and current at the initial segment of the wire are V_o and I_o, respectively. As current passes through the wire, the amount of current decreases in both longitudinal and radial axis because of leakage current through the wall (i_w) and the voltage drop along the wire. That is, the leakage current through the wire wall i_w and the axial current i_a decreases along the length of the wire. Graph (B) is an electrically equivalent circuit for the single wire within a conductive medium, where r_a is a resistor of each small segment along the cable axial direction, r_{cw} and r_m are the cable wall resistor and surrounding medium resistor of that segment, respectively. At a distance g, the axial and the wall current are assumed to be i_{ag} and i_{wg}, and the voltage is V(g). Ground (GND) cylinder is set at a finite distance (r_{gn} is the radial distance of the ground cylinder from the center of the wire) in the external medium.

The derivation of field potential distribution in a plane perpendicular to the wire is divided into following two steps:

A) Potential along the longitudinal axis of the wire (V_g)

From Ohm's law, which indicates that the voltage across a resistor is equal to the product of the resistance and the passing current,

a. axial current : $-\frac{dV_g}{dg} = r_a \cdot i_a$, (6.1)

b. wall leakage current : $-\frac{di_a}{dg} = i_{wg} = \frac{V_g}{r_w}$, (6.2)

where

i_{wg} = leakage current through the wire wall at the segment of distance g from the initial segment of the wire;

i_{ag} = axial current along the wire at the segment of distance l from the initial segment of the wire;

r_w = $r_{cw}+r_m$, is the wall resistance per unit length (Ω·cm) through the cable wall (r_{cw}) and medium (r_m); and r_a is axial resistance per unit length (Ω/cm).

From Equation 6.1 and 6.2, we get,

$$\frac{d^2V_g}{dg^2} = r_a \cdot i_{wg}$$

$$\frac{d^2V_g}{dg^2} = \frac{r_a \cdot V_g}{r_w}$$

$$\frac{d^2V_g}{dg^2} = V_g \cdot \frac{r_a}{r_w} \quad . \qquad (6.3)$$

Laplace transform is used to solve this cable Equation 6.3,

$$V(g)=A\cdot\exp(-\sqrt{C}\cdot g)+B\cdot\exp(\sqrt{C}\cdot g), \qquad (6.4)$$

where C is a constant (= r_a/r_w). The boundary conditions are,

1) when g=0, $V(g)=V_o$,

2) when $g \rightarrow \infty$, $V(g) \rightarrow 0$.

Therefore,

$$V(g)=V_0 \cdot \exp(-\sqrt{C} \cdot g)$$

$$V(g)=V_0 \cdot \exp(-g/\lambda), \qquad (6.5)$$

where $\lambda=1/\sqrt{C}=\sqrt{r_w/r_a}$, is the electrotonic length of the wire, and λ can be obtained experimentally (Katz, 1966). Equation 6.5 indicates that the potential drops along the longitudinal axis exponentially.

B) Potential in a plane at a single segment of the wire

A single element of the wire is shown in Figure 6.2, with length h and distance g from the initial segment. i_{wg} is the wall leakage current at segment g.

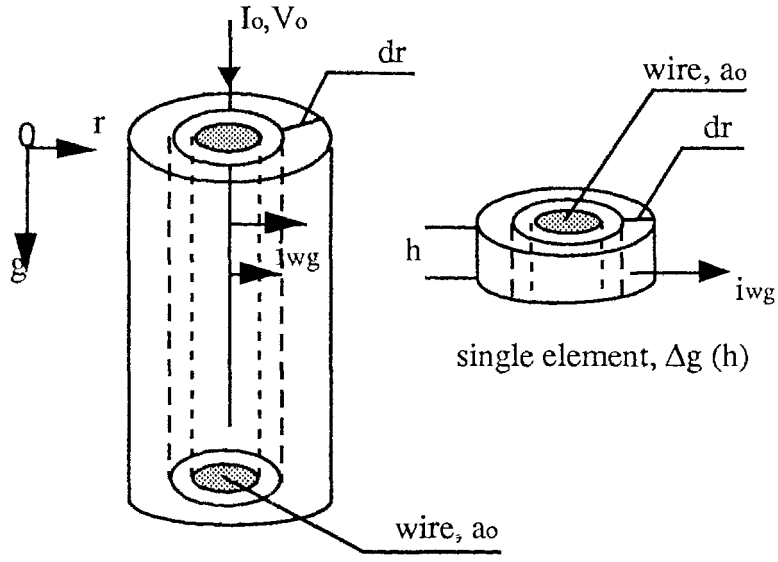

Figure 6.2 A single small segment of a wire The figure shows a long wire and a single small element of the wire Δg. I_o and V_o are initial current and voltage applied at the initial part of the wire. i_{wg} is the wall leakage current at segment g (which is the distance of the segment from the initial part), h is the length of the segment, a_o was the radius of the wire, and dr represented an infinitesimal distance between two cylinders in the medium.

For a unidirectional current source i_{wl}, based on the definition of resistance R, we have,

$$dR = \rho_m \cdot \frac{dr}{2\pi rh},$$

where ρ_m is the resistivity of the medium. According to Ohm's law,

$$\begin{aligned} dV_g &= i_{wg} \cdot dR \\ &= \frac{i_{wg} \cdot \rho_m \cdot dr}{2\pi rh} \\ &= \frac{i \cdot K \cdot dr}{r}, \end{aligned}$$

where $K=\rho/2\pi h$, is a constant. Then,

$$\int dV_g = \int \frac{i_{wg} \cdot K \cdot dr}{r}$$

$$V_{g,r} = i_{wg} \cdot K \cdot \ln r + C, \qquad (6.6)$$

where

K, C = constants decided from boundary conditions;

g = distance of the point away from the initial point of the wire;

r = distance of the point away from the center of wire.

From Equation 6.2 and 6.5,

$$\begin{aligned} i_{wg} &= \frac{V_g}{r_w} \\ &= \frac{V_0 \cdot \exp(-g/\lambda)}{r_w}. \end{aligned} \qquad (6.7)$$

The boundary conditions are:

a) when $r=a_o$, $V_{g,ao}=V_o \cdot \exp(-g/\lambda)$,

b) when $r=r_{gn}$ (Ground), $V_{l,rgn}=0$.

Substituting them into the Equation 6.6, two simultaneous equations can be obtained:

$$\begin{cases} V_o \cdot \dfrac{\exp(\frac{-g}{\lambda})}{r_w} \cdot K \cdot \ln(a_o) + C = V_o \cdot \exp(\frac{-g}{\lambda}) \\ V_o \cdot \dfrac{\exp(\frac{-g}{\lambda})}{r_w} \cdot K \cdot \ln(r_{gn}) + C = 0 \end{cases} . \qquad (6.8)$$

The solution is, $C = -V_o \cdot \dfrac{\exp(-g/\lambda)}{\ln(a_o/r_{gn})} \cdot \ln(r_{gn})$, and $K = \dfrac{r_w}{\ln(a_o/r_{gn})}$. Then,

$$\begin{aligned} V_{g,r} &= i_g \cdot K \cdot \ln r + C \\ &= V_o \cdot \frac{\exp(-g/\lambda)}{r_w} \cdot \frac{r_w}{\ln(a_o/r_{gn})} \cdot \ln r - \frac{V_o \cdot \exp(-g/\lambda)}{\ln(a_o/r_{gn})} \cdot \ln(r_{gn}) \\ &= \frac{V_o \cdot \exp(-g/\lambda)}{\ln(a_o/r_{gn})} \cdot \ln(r/r_{gn}). \end{aligned} \qquad (6.9)$$

The ground is usually outside the wire (i.e. $r_{gn} \geq a_o$), thus $V_{g,r}$ decreases as r increases, which suggests that the potential decays by ln(1/r) along the radial axis of a wire segment.

CHAPTER 7 REFERENCES

Andersen, P., Gjerstad, L. and Langmoen, I.A.I. (1978) A cortical epilepsy model in vitro. In: N. Chalazonitis and M. Boisson (eds), Abnormal Neuronal Discharges. Raven Press, New York: 29-36.

Andersen, T.E. and Rutledge, L.T. (1979) Inhibition in penicillin-induced foci Electroenceph. Clin. Neurophysiol., 46: 498-509.

Arvanitaki, A. (1942) Effects evoked in an axon by the activity of a contiguous one J. Neurophys. vol. 5, pp. 89-108, 1942.

Brown, T.H. and Johnston, D. (1983) Voltage-clamp analysis of mossy fiber synaptic input to hippocampal neurons Jnl. Neurophysiol. Vol.50, No.2, Aug. 1983.

Chusid, J.G. (1976) Correlative Neuroanatomy and Functional Neurology 16th. ed., LANGE Medical Publication.

Cutler, W.D. and Young, J. (1979) The effect of penicillin on the release of gamma-aminobutyric acid from cerebral cortex slices Brain Res., 170: 157-163.

Daniel, C., Wood, F.S. (1980) Fitting Equations to Data Computer analysis of multifactor data John Wiley & Sons, Inc., New York, USA.

Delgado-Escueta, A.V., M.D., Ward, A.A. Jr, M.D. *et al* (Editors) (1986) Basic Mechanisms of the Epilepsies--Molecular and Cellular Approaches in "Advances in Neurology" Vol.44 p.3.

Dingledine, R. and Gjerstad, L. (1980) Reduced inhibition during epileptiform activity in the in vitro hippocampal slice J. Physiol. (Lond.), 305: 297-313.

Ferris, Clifford D. (1974) Introduction to Bioelectrodes Plenum Press, New York, USA.

Futamachi, K.S. and Prince, D.A. (1975) Effect of penicillin on an excitatory synapse Brain Res. 100: 589-597.

Geddes, L.A. (1972) Electrodes and the Measurement of Bioelectric Events John Wiley & Sons, Inc., New York, USA.

Haas, H.L. and Jefferys, J.G.R. (1984) Low calcium field burst discharges of CA1 pyramidal neurons in rat hippocampal slices J. Physiol., 354: 185-201.

Jackson, J.H. (1870) A study of convulsions Trans. St. Andrews Med. Grad. Assn., 3:1-45.

Jasper, H., Ward, A. *et al* (Editors) (1969) Basic Mechanisms of the Epilepsies J. & A. Churchill Ltd., London.

Jefferys, J.G.R. (1981) Influence of electric fields on the excitability of granule cells in guinea-pig hippocampal slices J. Physiology (Lond.) 319 (1981): 143-152.

Jefferys, J.G.R. and Haas, H.L. (1982) Synchronized bursting of CA1 hippocampal pyramidal cells in the absence of synaptic transmission Nature, Lond. 300: 448-450.

Johnston, D. and Brown, T.H. (1983) Interpretation of voltage clamp measurements in hippocampal neurons Jnl. Neurophysiol. Vol.50, No.2, Aug. 1983.

Joyner, R.W., Moore, J.W. and Ramon, F. (1975) Axon voltage-clamp simulations III--- Postsynaptic Region Biophysical Jnl., Vol.15: 37-54, 1975.

Jung, Walter G. (1974) IC OP-amp Cookbook Howard W. Sams & Co. Inc. Indianapolis, Indiana, USA.

Kandel, E.R. and Schwartz, J.H. (1985) Principles of Neural Science. 2nd. ed., Elsevier, New York.

Katz, Bernard (1966) Nerve, muscle and synapse New York: McGraw-Hill, P. 73-75.

Katz, G.M. and Schwartz, T.L. (1974) Temporal control of voltage-clamped membranes: an examination of principles J. Membr. Biol. 17: 275-291, 1974.

Konnerth, A., Heinemann, U. and Yaari, Y. (1986) Nonsynaptic epileptogenesis in the mammalian hippocampus in vitro I. Development of seizurelike activity in low extracellular calcium J. Neurophysiol. Vol. 56, No. 2: 409-423.

Noebels, J.L. and Prince, D.A. (1978) Development of focal seizures in cerebral cortex: role of axon terminal bursting J. Neurophysiol. 41: 1267-1281.

Plonsey, R. and Barr, R.C. (1988) Bioelectricity--A Quantitative Approach Plenum Press, N.Y. & Lond. Chapt. 2.

Ramon, F. and Moore, J.W. (1978) Ephaptic transmission in squid giant axons 0363-6143/78 Ame. Physiol. Soc.:c162-c169 (1978).

Richardson, T.L., Turner, R.W., and Miller, J.J. (1984) Extracellular fields influence transmembrane potential and synchronization of hippocampal neuronal activity Brain Res. 294(1984): 255-262.

Scott, William T. (1959) The Physics of Electricity and Magnetism John Wiley & Sons, Inc.

Shepherd, G.M. (1979) The Synaptic Organization of the Brain 2nd. ed., Oxford University Press, N.Y. & Oxford.

Smith, T.G., Jr, Lecar, H. *et al* (Editors) (1985) Voltage and Patch Clamping with Microelectrodes The Williams & Wilkins Company, Baltimore, Maryland, U.S.A.

Suthorland, John M. and Eadie, Mervyn J. (1980) The Epilepsies (modern diagnosis and treatment) 3rd. Ed. Churchill Livingstone P. 2.

Taylor, C.P. and Dudek, F.E. (1982) Synchronous neuronal afterdischarges in rat hippocampal slices without active chemical synapses Science, N. Y. 218: 810-812.

Taylor, C.P. and Dudek, F.E. (1984a) Excitation of hippocampal pyramidal cells by an electrical field effect J. Neurophysiol. Vol.52, No.1: 126-142.

Taylor, C.P. and Dudek, F.E. (1984b) Synchronization without active chemical synapses during hippocampal afterdischarges J. Neurophysiol. Vol.52, No.1: 143-155.

Taylor, C.P., Krnjevic.K. and Ropert, N. (1984) Facilitation of hippocampal CA3 pyramidal cell firing by electrical fields generated antidromically Neuroscience Vol.11, No.1 pp. 101-109 (1984).

Turner, R.W., Richardson, T.L., and Miller,J.J. (1984) Ephaptic interaction contribute to paired pulse and frequency potentiation of hippocampal field potentials Exp. Brain Res. (1984) 54: 567-570.

Wong, R.K.S. and Prince, D.A. (1978) Participation of calcium spikes during intrinsic burst firing in hippocampal neurons Brain Res. 159: 385-390.

Wong, R.K.S. and Prince, D.A. (1979) Dendritic mechanisms underlying penicillin-induced epileptiform activity Science 204: 1228-1231.

Yaari, Y., Konnerth, A. and Heinemann, U. (1983) Spontaneous epileptiform activity of CA1 hippocampal neurons in low extracellular calcium solutions Exp. Brain Res., 51: 153-156.

Yaari, Y., Konnerth, A. and Heinemann, U. (1986) Nonsynaptic epileptogenesis in the mammalian hippocampus in vitro. II. Role of extracellular potassium Vol. 56, No. 2: 424-438.